https://doi.org/10.5194/acp-2020-1136
Preprint. Discussion started: 10 November 2020

Atmospheric Chemistry and Physics Discussions

Large and increasing methane emissions from Eastern Amazonia derived from satellite data, 2010 - 2018

Chris Wilson[1,2], Martyn P. Chipperfield[1,2], Manuel Gloor[3], Robert J. Parker[4,5], Hartmut Boesch[4,5], Joey McNorton[6], Luciana V. Gatti[7], John B. Miller[8], Luana S. Basso[7], Sarah A. Monks[9,10,*]

[1]National Centre for Earth Observation, University of Leeds, Leeds, UK
[2]School of Earth and Environment, University of Leeds, UK
[3]School of Geography, University of Leeds, Leeds, UK
[4]Earth Observation Science, School of Physics and Astronomy, University of Leicester, Leicester, UK.
[5]National Centre for Earth Observation, University of Leicester, Leicester, UK
[6]European Centre for Medium-Range Weather Forecasts, Reading, UK
[7]Earth System Science Center (CCST), National Institute for Space Research (INPE), Av. Dos Astronautas, 1758, 12.227-010, São José dos Campos, SP, Brazil
[8]Global Monitoring Laboratory, National Oceanic and Atmospheric Administration, Boulder, Colorado, USA
[9,*]Formerly at CIRES, University of Colorado Boulder, Boulder, CO, USA
[10,*]Formerly at Chemical Sciences Division, NOAA, Earth System Research Laboratory, Boulder, CO, USA

Correspondence to: Chris Wilson (c.wilson@leeds.ac.uk)

Abstract. We use a global inverse model, satellite data and flask measurements to estimate methane (CH_4) emissions from South America, Brazil and the basin of the Amazon River for the period 2010 – 2018. We find that emissions from Brazil have risen during this period, most quickly in the Eastern Amazon Basin, and that this concurrent with increasing surface temperatures in this region. Brazilian CH_4 emissions rose from 49.8 ± 5.4 Tg(CH_4)/yr in 2010 – 2013 to 55.6 ± 5.2 Tg(CH_4)/yr in 2014 – 2017, with the wet season of December – March having the largest positive trend in emissions. We derive no significant trend in regional emissions from fossil fuels during this period. We find that our posterior distribution of emissions within South America is significantly and consistently changed from our prior estimates, with the strongest emission sources being in the far north of the continent and to the south and south-east of the Amazon Basin, near the mouth of the Amazon and in other wetland regions. We derive particularly large emissions during the wet season of 2013/14, when flooding was prevalent over larger regions than normal within the Amazon Basin. We compare our posterior CH_4 mole fractions, derived from posterior fluxes, to independent observations of CH_4 mole fraction taken at five lower to mid tropospheric vertical profiling sites over the Amazon and find that our posterior fluxes outperform prior fluxes at all locations. In particular the large emissions from the eastern Basin are shown to be in good agreement with independent observations made at Santarém, a location which has long displayed higher mole fractions of atmospheric CH_4 in contrast with other Basin locations. We show that a bottom-up flux model cannot match the variation in annual fluxes, nor the positive trend in emissions, produced by the inversion. Our results show that the Amazon alone was responsible for 24 ± 18% of the total global increase in CH_4 flux during the study period, and it may contribute further in future due to its sensitivity to temperature changes.

https://doi.org/10.5194/acp-2020-1136
Preprint. Discussion started: 10 November 2020

1 Introduction

Methane (CH_4), a strong greenhouse gas emitted from a variety of anthropogenic and natural sources, is second only to carbon dioxide (CO_2) in its importance regarding the anthropogenic radiative forcing contributing to Earth's climate change (Myhre et al., 2013). Much of the CH_4 that is emitted into the atmosphere is destroyed through reaction with the hydroxyl (OH) radical and other smaller sinks, but a net positive imbalance means that the atmospheric burden of CH_4 has been increasing steadily since preindustrial times (e.g. Rubino et al., 2019). With an atmospheric lifetime of approximately 9 years (Prather et al., 2012), CH_4 is a potentially important species for short-term gains in mitigation of anthropogenic climate change (Shindell et al., 2012). However, the magnitude of the global sources of CH_4 to the atmosphere, and of its sinks once in the atmosphere, are still not well quantified (Saunois et al., 2020). The geographical distribution and sectoral attribution of methane emissions, and the inter-annual variation of these sources, are also uncertain (Saunois et al., 2016; Schaefer, 2019). This leads to difficulties in assessing potential emission mitigation strategies, hampering our ability to meet and assess the criteria for limiting the global temperature increase put forward as part of the Paris climate agreement (Nisbet et al., 2019).

The atmospheric methane burden is now approximately 2.5 times higher than it was in 1750 (Rubino et al., 2019). The global mean burden stabilised between 2000 and 2007, after which it began increasing again (Nisbet et al., 2016). Concerningly, the rate of increase of the atmospheric burden has accelerated since 2014 (Nisbet et al., 2019). This suggests that CH_4 emissions have been increasing at an accelerated rate during the past decade, but our understanding of how emissions are changing is complicated by the following:

(1) attributing a potential emission increase to a particular region and/or sector is complex, leading to conflicting hypotheses regarding the changing fluxes (e.g. Nisbet et al., 2016; Worden et al., 2017; Monks et al., 2018; Schaefer, 2019; Lan et al., 2019; Jackson et al., 2020);

(2) the uncertainty surrounding the distribution and variation of tropospheric OH means that variations in this major atmospheric sink of methane might also have played some role in the stabilisation and renewed rise (McNorton et al., 2016; Rigby et al., 2017; Turner et al., 2017; McNorton et al., 2018); and,

(3) whilst rising atmospheric mole fractions of many greenhouse gases signify increasing anthropogenic influence, the changing isotopic signature of atmospheric CH_4 as the burden rises appears to indicate that fossil fuel emissions are not the main contributors to the increase, and that other sectors could be responsible (Schaefer et al., 2016; Nisbet et al., 2019; Fujita et al., 2020), including anthropogenic agricultural emissions. However, it has been argued that increasing fossil fuel emissions could still be reconciled with the observed isotopic signature (Worden et al., 2017; Howarth, 2019).

In general, anthropogenic emissions of CH_4 from fossil fuels, agriculture and waste are better constrained than natural emissions, particularly in bottom-up inventories (Saunois et al., 2020). The majority of natural emissions come from wetlands, with smaller contributions from inland freshwaters, oceans, termites, wild animals and geological seeps. There are

https://doi.org/10.5194/acp-2020-1136
Preprint. Discussion started: 10 November 2020

also small but significant emissions from biomass burning, which are sometimes counted separately from other anthropogenic emissions despite often being due to agricultural land clearing (van der Werf et al., 2017).

Wetlands are the largest single-sector contributors to the global methane flux (Saunois et al., 2020) and the basin of the Amazon river in South America, covering an area of approximately 6,000,000 km^2 (Poulter et al., 2010), is a significant contributor to the global wetland CH_4 emission budget (Wilson et al., 2016; Bloom et al., 2017). The majority of the Basin is within the borders of Brazil. There are also a number of other significant wetland sources within South America, and often significant contributions from fires during warmer, drier years (van der Werf et al., 2017). Recent studies have suggested that there is also a direct contribution from trees in the Amazon, although there is likely some overlap with wetland fluxes in some inventories (Pangala et al., 2017). In fact, the contribution of each of these sources of CH_4, along with their regional distribution and variance over time, is still relatively uncertain. Earlier estimates of CH_4 emissions from the Amazon Basin ranged from 4 to 92 Tg(CH_4)/yr (Melack et al., 2004; do Carmo et al., 2006; Kirschke et al., 2013), but recently estimates have converged somewhat, e.g. 31.6 – 41.1 Tg/yr (Wilson et al., 2016), 42.7 ± 5.6 Tg /yr (including tree flux) (Pangala et al., 2017) and 44.4 ± 4.8 Tg yr (Ringeval et al., 2014). The global wetland total was recently estimated to be 148 ± 25 Tg(CH_4)/yr from bottom-up estimates and 159 – 200 Tg(CH_4)/yr from top-down models (Saunois et al., 2020), which implies that if the majority of the emissions from the Amazon are from wetlands, then the region contributes up to ~30% of the global CH_4 wetland flux.

Many studies have attempted to estimate national CH_4 emissions rather than from ecosystems such as the Amazon, partly as it will likely be easier for countries to put in place emission reduction protocols on a national basis. Some recent studies have therefore reported emission totals for the country of Brazil. The synthesis of Saunois et al. (2020) used a suite of top-down models to find a wide range of 47.3 – 78.2 Tg(CH_4)/yr total emissions from all sources within Brazil during the period 2008 – 2017. Natural sources made up 26.9 – 53.8 Tg(CH_4)/yr of this total. Janardanan et al. (2020) used a global inversion to constrain total Brazilian emissions to 56.2 ± 10 Tg(CH_4)/yr in the period 2011-2017. However, Tunnicliffe et al. (2020) used a high-resolution regional inversion to find much smaller emissions from the country, calculating total Brazilian emissions of 33.6 ± 3.6 Tg(CH_4)/yr, with wetlands making up 13.0 ± 1.9 Tg(CH_4)/yr of this total. The relatively large range of estimates produced by these studies, some of which make use of the same observational datasets, is indicative of the difficulties inherent in using top-down methods to assess surface emissions of CH_4 from within the poorly monitored continent of South America. However, in order to best understand the global methane budget and its sources, it is still vital that the significant contribution of South American emissions is evaluated and attributed.

In order to best unite these estimates, regular observation of atmospheric methane over South America is necessary. The Thermal And Near infrared Sensor for carbon Observations – Fourier Transform Spectrometer (TANSO-FTS) instrument on

https://doi.org/10.5194/acp-2020-1136
Preprint. Discussion started: 10 November 2020

the GOSAT satellite (Kuze et al., 2009) is particularly advantageous, as it is sensitive far down into the troposphere and has been providing regular global coverage of atmospheric CH_4 continuously since April 2009 (Parker et al., 2020a). This decade of uninterrupted global coverage allows for understanding of methane variations over a much longer time period than many of the other available datasets, particularly in the tropics.

In this paper we use CH_4 observations from GOSAT along with flask measurements both from within and outside the Amazon Basin to provide an almost complete 10-year record of methane emissions from South America, beginning in 2009. We use the TOMCAT chemical transport model and its inverse model, INVICAT, to quantify emissions and their uncertainties during this decade. Ours aims are to 1) assess the geographical distribution of South American CH_4 emissions, with focus on the country of Brazil and the Amazon Basin ecosystem; 2) examine how these emissions have changed during the previous decade; and 3) investigate why any changes to natural emissions might have occurred. We describe the observations used and the modelling methodology in Section 2. We show our results and discuss our findings in Section 3 and Section 4, respectively.

2 Methods

2.1 Observations

We assimilate both in-situ flask observations and GOSAT satellite retrievals of CH_4 into the inverse model. We also hold back a set of observations made as part of regular flask-based aircraft monitoring campaign within the Amazon Basin since 2010, for validation of our results.

2.1.1 Surface flask observations

We assimilate global long-term surface data of CH_4 provided by the National Oceanic and Atmospheric Administration's Global Monitoring Laboratory (NOAA GML) (Table A4). We use data from 56 background monitoring sites, the locations of which are shown in Figure 1. Whole air samples in flasks are collected weekly to biweekly at each site, and CH_4 is measured using gas chromatography with a flame ionization detection method (Dlugokencky et al., 2018). Data from these sites is assimilated in order to constrain the background variations in CH_4 mole fractions at the Earth's surface. The observations made at these locations have high accuracy but are generally located in regions that are not near significant sources of CH_4. There is also a relative lack of regular observations in tropical regions, where CH_4 emissions are significant and uncertain. This means that these observations can provide accurate values for background CH_4 values but are not usually able to provide accurate regional CH_4 distributions in those areas that require the most constraint.

https://doi.org/10.5194/acp-2020-1136
Preprint. Discussion started: 10 November 2020

2.1.2 GOSAT observations

We also assimilate column-averaged dry-air mole fractions of CH_4 (XCH_4) from the University of Leicester Proxy retrieval scheme v7.2 for GOSAT (Parker et al., 2011, 2020a). This dataset has been used in the past in forward modelling studies to assess wetland CH_4 emissions using the TOMCAT model (Parker et al., 2018, 2020b). The GOSAT Proxy scheme uses the ratio of the retrieved XCO_2 and XCH_4, together with model-based estimates of XCO_2, in order to reduce the effects of atmospheric scattering and improve coverage of XCH_4 retrievals. This is particularly true in tropical land regions where the prevalence of cloudy pixels often restricts the successful direct retrieval of XCH_4. GOSAT XCH_4 retrievals have been used previously in a number of forward and inverse modelling studies (Fraser et al., 2013; McNorton et al., 2016; Feng et al., 2017; Miller et al., 2019). The observations are regularly validated against independent data, including CH_4 observations made as part of the Total Carbon Column Observing Network (TCCON, Wunch et al., (2011)), although unfortunately none of the measurement sites included as part of this network are located within the Amazon region. Webb et al. (2016) compared GOSAT XCH_4 to vertical profile observations of CH_4 taken over the Amazon Basin and found that the two agreed within their respective errors.

Before assimilation, GOSAT observations were averaged onto the model grid. Both sun-glint observations over the oceans and nadir observations over land were included in the inversion. All XCH_4 values measured by the satellite during one model timestep in the same grid cell were averaged using a weighted mean according to their uncertainties. The largest number of observations combined into a single value was 32, and the mean number was 4.7 over land and 6.0 over oceans. Within the Amazon Basin, the mean number of observations combined was 3.8. Figure 1 shows an example monthly distribution of observations used in the inversion. For accurate comparison between the retrieved XCH_4 and those simulated by the model, the GOSAT averaging kernels were averaged similarly to the XCH_4 and applied to the model vertical profiles. This meant that the adjoint code for this process was also produced for this study. Retrievals for which the model and satellite surface pressure differed by more than 50 hPa were rejected.

Due to a range of potential error sources in both the atmospheric transport model and the GOSAT retrievals, there is a persistent bias between them, which varies with latitude. We quantified this bias by comparing the results of a previous inversion, in which only the surface flask observations had been assimilated for the full 2009-2018 period, to the GOSAT XCH_4. We applied the averaging kernels to the three-dimensional (3-D) CH_4 output from the flask data inversion and calculated the model – observation zonal mean bias $B(\varphi)$, in parts per billion (ppb), as a function of latitude (φ), over this period:

$$B(\varphi) = 0.0016\varphi^2 - 0.1\varphi + 4.4\,, \qquad (1)$$

https://doi.org/10.5194/acp-2020-1136
Preprint. Discussion started: 10 November 2020

where φ is equal to the latitude of the observation in degrees north. Positive values of $B(\varphi)$ indicate positive observation bias relative to the model. Across the tropics (30°S – 30°N), the derived bias varies between 2.8 and 8.8 ppb. Further south, the bias reaches values up to 13.4 ppb. In the analysis below we add the estimated bias value to the simulated XCH_4 values in the inversion after the averaging kernels are applied.

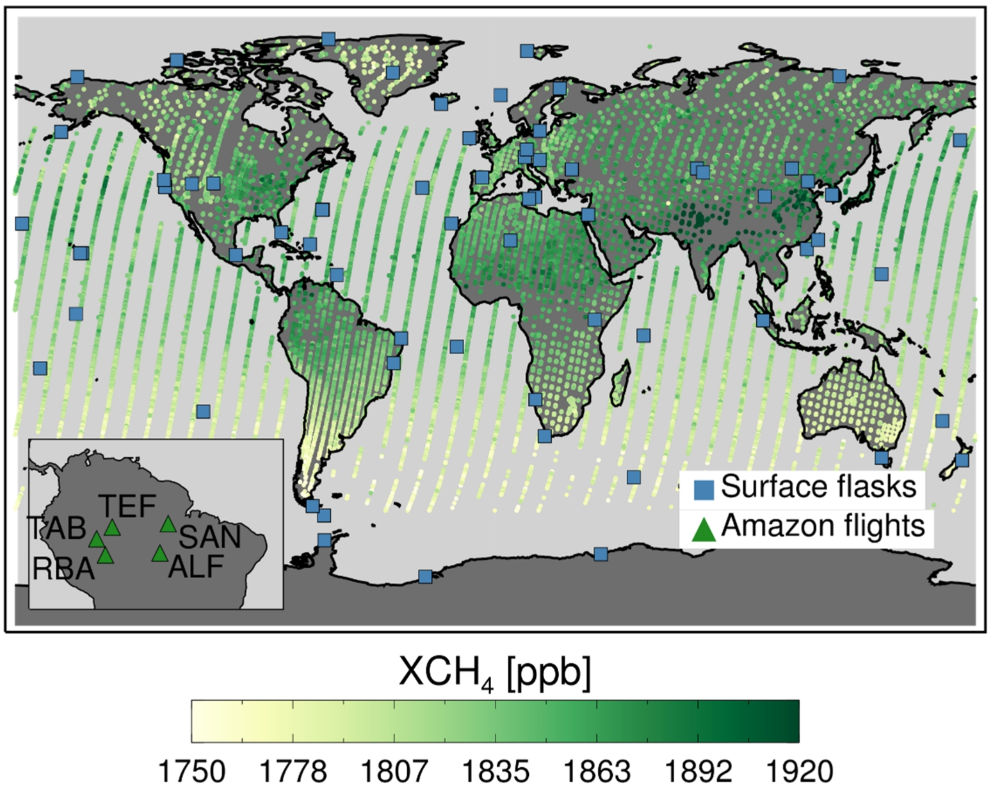

Figure 1: Locations of NOAA surface sites from which flask-based measurements of CH_4 are assimilated (blue squares), along with locations and values of GOSAT XCH_4 retrievals for August 2017 (circles). Inset shows locations of flight-based observations of CH_4 within the Amazon Basin (green triangles).

2.1.3 Amazonian aircraft profiles

Since 2010, aircraft-borne flask air observations of a number of species, including CH_4, CO_2 and carbon monoxide (CO) have been made at five locations within the Amazon Basin (shown in Figure 1) by researchers at the Instituto de Pesquisas Energéticas e Nucleares (IPEN) in Sao Paulo, Brazil (until 2014) and at the National Institute for Space Research (INPE) Sao Jose dos Campos, Brazil (since 2015). The sites are located at Santarem (SAN, 55.0°W, 2.9°S), Tabatinga (TAB, 69.7°W, 6.0°S), Alta Floresta (ALF, 56.7°W, 8.9°S), Rio Branco (RBA, 67.9°W, 9.3°S) and Tefé (TEF, 66.5°W 3.6°S).

https://doi.org/10.5194/acp-2020-1136
Preprint. Discussion started: 10 November 2020

Measurements were only ever made concurrently at four locations, as the measurements at Tefé were started in 2013, to replace those made at Tabatinga up to 2012. We therefore combine observations made at these locations and refer to them as TAB/TEF throughout this manuscript. Both sites are located in the north-west of the Amazon Basin and sample similar air masses. Flights are undertaken at approximately biweekly intervals above each site up to an altitude of ~4.4 km, and 0.7 L flasks were filled every 300–500m to produce vertical profiles. All measurements were taken between 12:00 and 13:00 local time, when the boundary layer is fully developed. The flasks were analysed for CH_4 mole fractions at the high-precision gas analytics laboratory at IPEN and INPE, following the NOAA GML approach, including rigorous calibration to the World Meteorological Organization (WMO) CH_4 mole fraction scale. The measurement locations were chosen in order to sample the dominant tropospheric airstream across the Basin. For more information about these measurements, see Gatti et al. (2014) and Basso et al. (2016).

2.2 Model set-up

2.2.1 Inverse model set-up

The TOMCAT model is a global 3-D Eulerian offline chemical transport model (CTM) (Chipperfield, 2006; Monks et al., 2017). It has been used in a number of previous studies of atmospheric composition and transport (e.g. Wilson et al., 2016; McNorton et al., 2016; Parker et al., 2018). We use the INVICAT inverse model (Wilson et al., 2014), which is based on the TOMCAT model. INVICAT uses a variational scheme based on 4D-Var methods used in Numerical Weather Prediction (NWP) and has been used in the past to constrain emissions of other species (Gloor et al., 2018; Monks et al., 2018; Thompson et al., 2019; Tian et al., 2020). The inverse method employed by INVICAT is described in depth in these previous references.

In this study, the forward and adjoint model simulations were carried out at 5.6° horizontal resolution, with 60 vertical levels up to 0.1 hPa. The model time step was 30 minutes. The meteorology was taken from the European Centre for Medium-Range Weather Forecasts (ECMWF) ERA-Interim reanalyses (ERA-I, Dee et al. (2011)). The inversions were carried out for each year separately and each completed 40 minimisation iterations. The inversion for each year was actually run for 14 months up to the end of February for the following year, with the final two months being discarded from the results. This was in order to better constrain fluxes during the final months of each year. Each inversion therefore overlapped with the following one for two months but was initialized using 3-D fields provided from the correct date in the previous year, so that total CH_4 burden was conserved across years.

For the assimilated surface observations, the model output was linearly interpolated to the correct longitude, latitude and altitude, at the nearest model timestep. For the averaged GOSAT observations, the model mole fractions were interpolated to the correct longitude and latitude at the nearest time step, before the GOSAT averaging kernels were applied to the model output to give an XCH_4 value comparable with GOSAT. GOSAT observations were given an uncorrelated uncertainty equal to 2.5 times the supplied retrieval error, which ranged from 3.5 to 25.8 ppb, in order to account for representation error and observation correlations removed by the averaging of the retrievals, as in Chevallier (2007). This inflation value was based on the mean number of observations combined in each grid cell. In short sensitivity tests, the magnitude of posterior emissions was not sensitive to this inflation factor once it was larger than 2, although the posterior error estimate was affected. This choice gave a mean GOSAT XCH_4 uncertainty value of 24.4 ppb. NOAA observations were given uncorrelated errors of 3 ppb plus representation error. For these observations, representation error was estimated as the mean difference across the 8 grid cells surrounding the cell containing the observation location.

Prior emissions were given grid cell uncertainties of 250%, but also included spatial and temporal correlations. Although inversions such as this do not directly allow for sectorial analysis of emissions, we used the off-diagonal values of the prior covariance matrix to provide some information of this nature. Similar to Meirink et al., (2008), we split out prior and posterior solutions into the anthropogenic fossil fuel emissions assumed to be strongly correlated in time (FF), and emissions with strong seasonal cycles from natural, agricultural and biomass burning sources (NAT + AGR + BB) by imposing prior temporal correlations on the FF contributions. FF emissions in each grid cell in each month were correlated with emissions from the same grid cell in other months with an exponential correlation time scale of 9.5 months (equivalent to a consecutive-month correlation of 0.9). Both NAT + AGR + BB and FF sectors had spatial correlations imposed with normal distributions and correlation length scales of 500km. This gives global uncertainty of approximately 70 Tg(CH_4)/yr. The sectors which make up the NAT + AGR + BB and FF emissions are explained in Section 2.2.2.

We produced estimates for each year's posterior emission covariance error matrix using the L-BFGS method (Nocedal, 1980) and updates suggested by Bousserez et al. (2015). This uses multiple iterations in order to estimate the inverse of the hessian (the second derivative) of the cost function, and does not include the off-diagonal elements of the posterior covariance matrix, so the posterior errors described in this manuscript are likely to be upper limits (Bousserez et al., 2015).

2.2.2 Prior emissions and chemical sinks of CH_4

Prior emissions were taken from a range of widely available bottom-up models and inventories. Anthropogenic emissions were originally taken from the EDGAR v4.2 FT 2010 inventory (Olivier et al., 2012) and scaled as in McNorton et al. (2018). Biomass burning emissions were taken from GFEDv4.2 (van der Werf et al., 2017). The JULES model (Clark et al., 2011) was used to provide wetland fluxes, in a configuration described in McNorton et al. (2016). Rice emissions were taken from Yan et al., (2009) and are scaled as in Patra et al. (2011). Remaining natural sources were included as in Wilson et al. (2016). The surface soil sink due to methanotrophs was from the Soil Methanotrophy Model (MeMo, Murguia-Flores et al., (2018)) and repeated the 2009 emission totals for every year. Landfill and fossil fuel emissions had temporal correlations imposed in the prior uncertainty matrix and made up the FF category, whilst the remaining emissions (NAT + AGR + BB) had no prior temporal correlations imposed. Prior totals for each source type within South American regions are shown in Table 1. Atmospheric OH fields, based on those provided within the TransCom CH_4 study (Patra et al., 2011) were taken from Spivakovsky et al. (2000) and scaled downwards by 8% in accordance with Huijnen et al. (2010). These vary from month to month but do not vary between years. Montzka et al. (2011) suggested that variability in annual OH mole fractions is small, but some recent research has suggested the possibility of a declining trend in OH since 2004 (Rigby et al., 2017; Turner et al., 2017), although this trend had a high level of uncertainty. A trend, or any significant year-to-year variability, in OH which was not included in our analysis, would affect our conclusions, but for now we do not have enough evidence to include any potential variations. Stratospheric loss fields due to reactions with atomic chlorine (Cl) and excited oxygen atoms (O^1D) varied on a monthly and annual basis and were taken from a previous full chemistry simulation from TOMCAT (Monks et al., 2017). Loss in the troposphere through reaction with chlorine was not included in these simulations.

2.2.3 Bottom-up model

We also use a simple bottom-up (B-U) model to estimate CH_4 emissions from climatological driving data, so that we can investigate the causes of variations in CH_4 emissions derived in the inversion. The B-U model calculates wetland CH_4 emissions based on the method used in Bloom et al. (2017), in which the CH_4 emissions in a grid cell, x, at time, t, are dependent on climatological factors as follows:

$$F(t,x) = s\,A(t,x)\,R(t,x)\,q_{10}^{\frac{T(t,x)}{10}}\,, \qquad (2)$$

where $F(t,x)$ is the flux of CH_4 in molecules cm^{-2} s^{-1}, $A(t,x)$ is the wetland fraction, $R(t,x)$ is the heterotrophic respiration of carbon per unit area, $T(t,x)$ is the surface temperature in °C, and q_{10} is the relative CH_4:C ratio of respiration for a 10°C change in temperature. Finally, s is a scaling factor. We use monthly mean values for each element of Eq. (2) and interpolate all parameters to the TOMCAT model grid for comparison with the inversion results.

We take R from the CASA-GFED v4.1 data product (Randerson et al., 2015), which runs up to 2016, and gridded 2m temperature from the NOAA/NCEP Global Historical Climatology Network version 2 and the Climate Anomaly Monitoring System GHCN Gridded V2 data provided by the NOAA Physical Sciences Laboratory (https://psl.noaa.gov/, Fan and Dool, (2008)). We estimate A using a combination of two products. We take a climatology of wetland fraction $w(x)$ from the JULES land surface model version that was used to produce the prior emissions used in the inversion (McNorton et al., 2016). We then use measurements of gravity anomalies made on the twin GRACE satellite mission, $G(t,x)$ as a proxy for variations in the soil moisture, as in (e.g.) Bloom et al. (2010) and Gloor et al. (2018). We then apply scaling factors a_1 and a_2 to give wetland fraction as follows:

https://doi.org/10.5194/acp-2020-1136
Preprint. Discussion started: 10 November 2020

Atmospheric Chemistry and Physics Discussions

$$A(t,x) = a_1 w(x) + a_2 G(t,x)\ , \tag{3}$$

This makes the assumption that anomalies in the gravity anomaly $G(t,x)$ are linearly related to wetland fraction anomalies, which may not be the case. The distributions and variations of the GRACE gravity anomalies and surface temperature are discussed in Section 4. We create an ensemble of B-U estimates for F, letting the scaling factors a_1 and a_2 and the temperature response function q_{10} vary within reasonable limits, and varying s appropriately so that each member gives the same mean total emissions over 2010 – 2017, equal to the mean posterior value produced by the inversion. We are interested only in the variations in time and space produced by the B-U model, rather than the absolute value. We let q_{10} vary between 1 and 3, based on experimental bounds and previous bottom-up studies of methane emissions (Yvon-Durocher et al., 2014; Bloom et al., 2017), we let a_1 vary between 0.8 and 1.2, and we let a_2 vary in such a way that the overall wetland fraction does not vary by more than 20%, depending on the value of a_1. Since there is no data for 2017 given for the heterotrophic respiration, we use a climatology made up from the preceding seven years applied to that year. We also create an 'optimised' B-U model, in which we use a curve-fitting procedure to choose values of s, a_1, a_2 and q_{10} which best fit, in least-squares terms, the results from the inversion for the monthly and spatial mean values over the whole Amazon, for all months within the wet season over 2010 - 2017. For this B-U model, we consider only the wet season NAT + AGR + BB emissions within the Amazon Basin, which we assume to be almost entirely from wetlands.

The equation that our B-U model is based on is commonly used in other studies which estimate wetland fluxes of CH_4 (e.g. Clark et al., 2011; Melton et al., 2013; Bloom et al., 2017), but our application of the driving climate variables is fairly simple relative to these previous works. This method is sufficient for this work as the purpose of the B-U model is to investigate the possibility of reproducing the inversion results, and if they can be reproduced, to learn how and why the CH_4 wetland emissions change according to the input variables.

3 Results

3.1 Average distribution of emissions

Average GOSAT XCH_4 over South America since 2009 show that XCH_4 column mole fractions were largest over the west of the continent, particularly in the northwest (Figure 2). Using the *a priori* emission distribution in TOMCAT leads the model to underestimate XCH_4 in the northeast and far north of the continent and in the outflow into the Atlantic Ocean. Simulated XCH_4 is overestimated to the south and west of the continent. After assimilating the observations, the largest positive and negative biases are removed across the continent, although there is a small positive model bias in the interior of the continent, usually smaller than 5 ppb. The posterior error-weighted mean residual model-satellite mismatch is 0.2 ppb

https://doi.org/10.5194/acp-2020-1136
Preprint. Discussion started: 10 November 2020

globally, -5.4 ppb within South America and -4.1 ppb within the Amazon Basin. The prior equivalents are -24.1 ppb, -40.0 ppb and -66.5 ppb, respectively. The posterior residuals show no significant trend or seasonality.

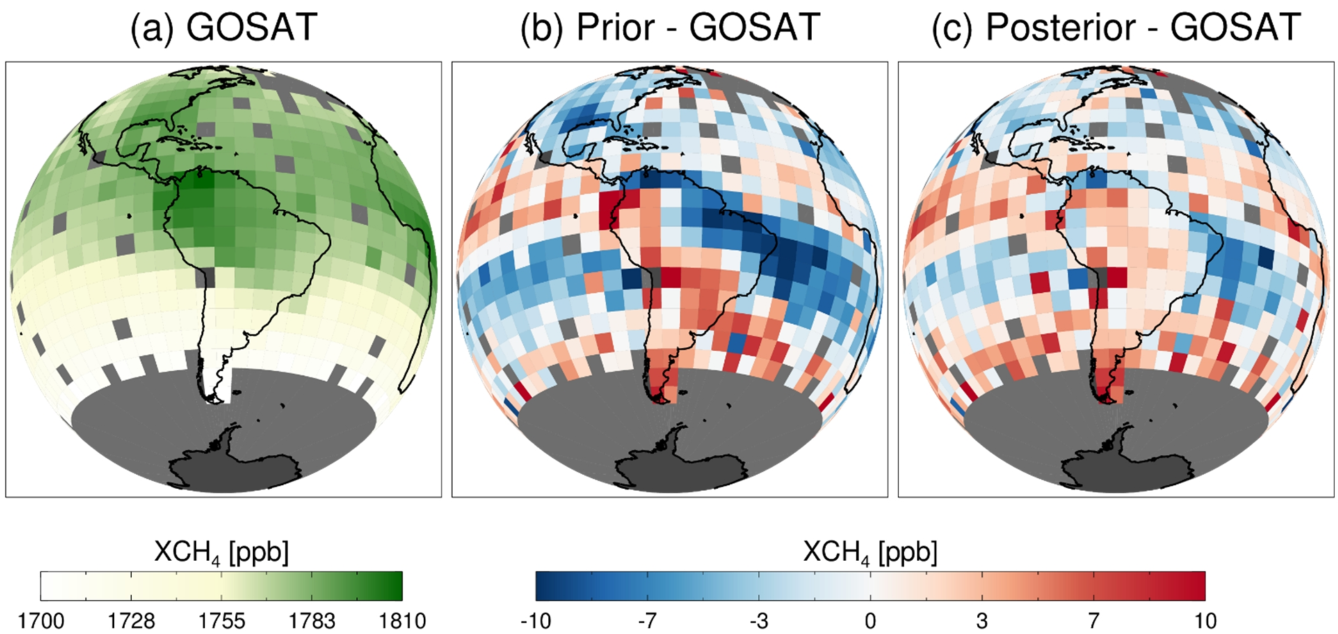

Figure 2: (a) Mean GOSAT XCH_4 over South America and surrounding area for 2009 - 2018. Observations have been averaged onto the TOMCAT model grid as described in the text. Also shown is the mean difference between the model and satellite XCH_4 using (b) the prior emissions and (c) the posterior emissions for the same period.

Figure 3 shows the 2009 – 2018 mean prior and posterior emission distributions of CH_4 emissions in South America. We display the mean over this entire period in order to show the consistent, long-term emission distribution. Posterior uncertainty in particular grid cells can still be fairly large, but regional changes are much less uncertain. Posterior South American emissions are significantly redistributed compared to the prior distribution and this is mainly due to changes in the NAT + AGR + BB emission sectors. Whilst the prior emissions are fairly homogeneous across much of the Brazilian Amazon, the posterior emissions are largest at the north-eastern side of the continent and are reduced in the south and the north-west. Emission rates in the far north of the continent remain high in the posterior estimate.

The most significant feature of the posterior distribution is a region of high emission rates near the coastal basins around the mouth of the Amazon River itself. There are significant emissions from the region around the north-eastern states of Para, Maranhão and Tocantins. These areas contain the basins of many of the larger Amazon tributaries and a high density of wetland sources such as marshes, swamps and mangroves, according to the Sustainable Wetlands Adaptation and Mitigation Program (SWAMP) data from the Center for International Forestry Research (CIFOR) (Gumbricht et al., 2017).

https://doi.org/10.5194/acp-2020-1136
Preprint. Discussion started: 10 November 2020

However, in our posterior results, the west of the Amazon Basin and the Pantanal region in the south of Brazil do not display high emissions. Although the coarse resolution of the model grid boxes masks the signal from the relatively small Pantanal region even in the prior emissions to some extent, it is still surprising that the posterior emissions would not have some significant methane flux from the southern regions of Brazil. As shown in Fig. 2, the model generally overestimates the XCH_4 is southern Brazil compared to GOSAT when using the prior emissions, so it is not surprising that emissions from that region were reduced in the inversion. The low emissions from a region where we expect significant methane release might mean that the model transport affects comparisons in this region in an unrealistic way, that the model-satellite bias included in the inversion (Eq. (1)) is inaccurate, or that the satellite retrievals are biased in this region. The relatively low emissions in the western Amazon are also a consistent feature of our results. The FF emissions do not change significantly in the inversion, although they are slightly decreased towards the south east of Brazil, close to the large cities of São Paulo and Rio de Janeiro. The overall pattern of the posterior emissions displayed in Figure 3 is robust on a year-to-year basis, with the change to the prior in each individual year displaying very similar patterns to the multi-year mean (Figure S1).

Table 1: Prior and posterior emissions of CH_4 for Brazil and other subregions of South America (2010 – 2017). Units are Tg(CH_4)/yr.

	Prior (Tg(CH_4)/yr)				**Posterior (Tg(CH_4)/yr)**			
	2010-2013		**2014-2017**		**2010-2013**		**2014-2017**	
	NAT + AGR + BB	**FF**	**NAT + AGR + BB**	**FF**	**NAT + AGR + BB**	**FF**	**NAT + AGR + BB**	**FF**
Brazil	38.9 ± 11.7	10.6 ± 9.2	38.2 ± 11.4	10.6 ± 9.2	39.9 ± 5.3	9.9 ± 0.9	45.7 ± 5.1	9.9 ± 0.9
South America	59.9 ± 16.4	23.9 ± 16.2	58.5 ± 16.0	23.9 ± 16.2	62.7 ± 7.0	31.6 ± 1.7	68.9 ± 6.7	28.9 ± 1.8
West Brazilian Amazon	10.1 ± 5.4	0.3 ± 0.5	10.2 ± 5.5	0.3 ± 0.5	9.7 ± 2.9	0.3 ± 0.0	12.0 ± 2.8	0.3 ± 0.0
East Brazilian Amazon	13.4 ± 7.1	2.7 ± 3.8	12.9 ± 6.7	2.7 ± 3.8	20.0 ± 3.4	2.4 ± 0.3	24.3 ± 3.3	2.5 ± 0.3
Non-Amazon Brazil	15.4 ± 6.3	7.5 ± 8.4	15.1 ± 6.2	7.5 ± 8.4	10.2 ± 2.9	7.2 ± 0.8	9.3 ± 2.8	7.1 ± 0.9
Amazon Basin	35.6 ± 12.4	4.1 ± 4.3	35.1 ± 12.2	4.1 ± 4.3	38.2 ± 5.3	3.5 ± 0.3	45.6 ± 5.2	3.7 ± 0.3

https://doi.org/10.5194/acp-2020-1136
Preprint. Discussion started: 10 November 2020

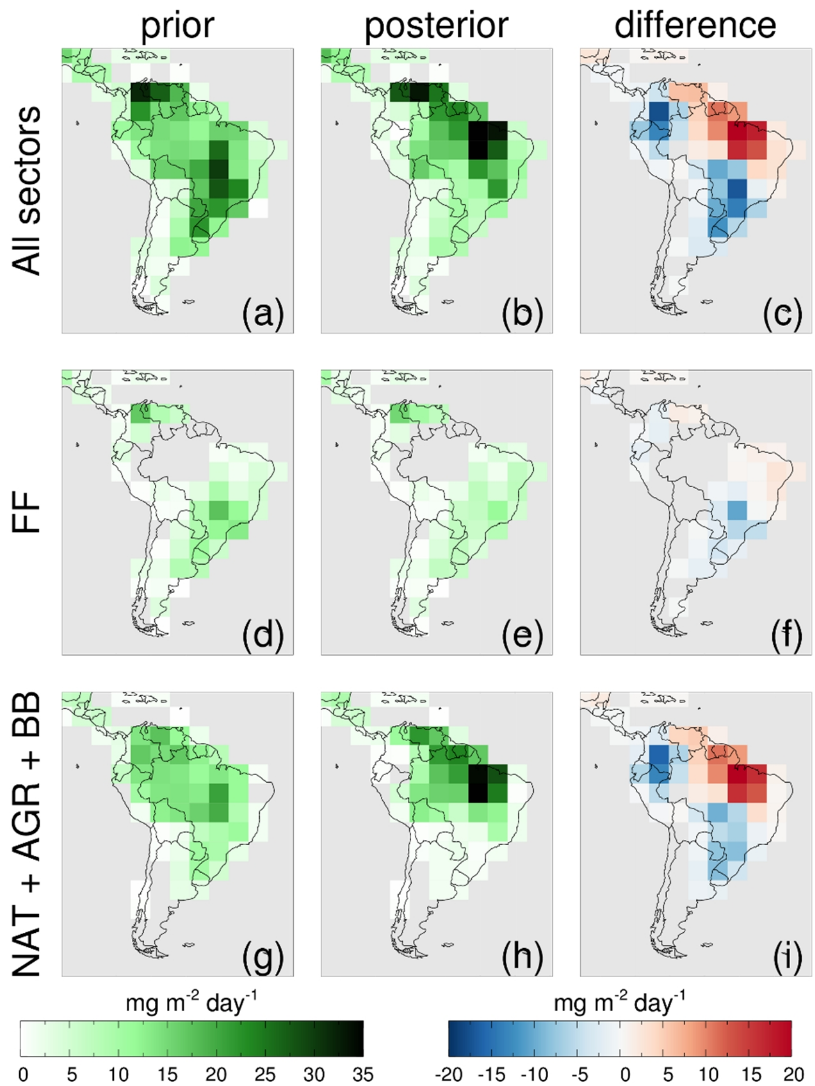

Figure 3: Prior, posterior and (prior – posterior) mean gridded total South American CH4 emissions (mg m^{-2} day^{-1}) for the period 2009 – 2018 (a-c), and similar but for fossil fuel sources (d-f) and natural/agricultural/biomass burning sources (g-i) only.

3.2 Temporal variations of CH_4 emissions

The annual total prior emissions in Brazil are consistent over time (Figure 4), with a mean value of 48.6 ± 14.9 Tg(CH_4)/yr. However, the posterior emissions show a positive trend, particularly from 2013 onwards. In the posterior results, the mean annual emissions are 49.8 ± 5.4 Tg(CH_4)/yr in the period 2009 – 2013, but rise to 55.6 ± 5.2 Tg(CH_4)/yr in 2014 – 2018, with a mean value over the whole period of 52.7 ± 5.3 Tg(CH_4)/yr. The uncertainty stated for these figures represents the overall mean annual posterior uncertainty for Brazil derived in the inversion for each 4-year period. We report the mean annual uncertainty as we assume that posterior uncertainty for each year is strongly correlated with that in other years. This

https://doi.org/10.5194/acp-2020-1136
Preprint. Discussion started: 10 November 2020

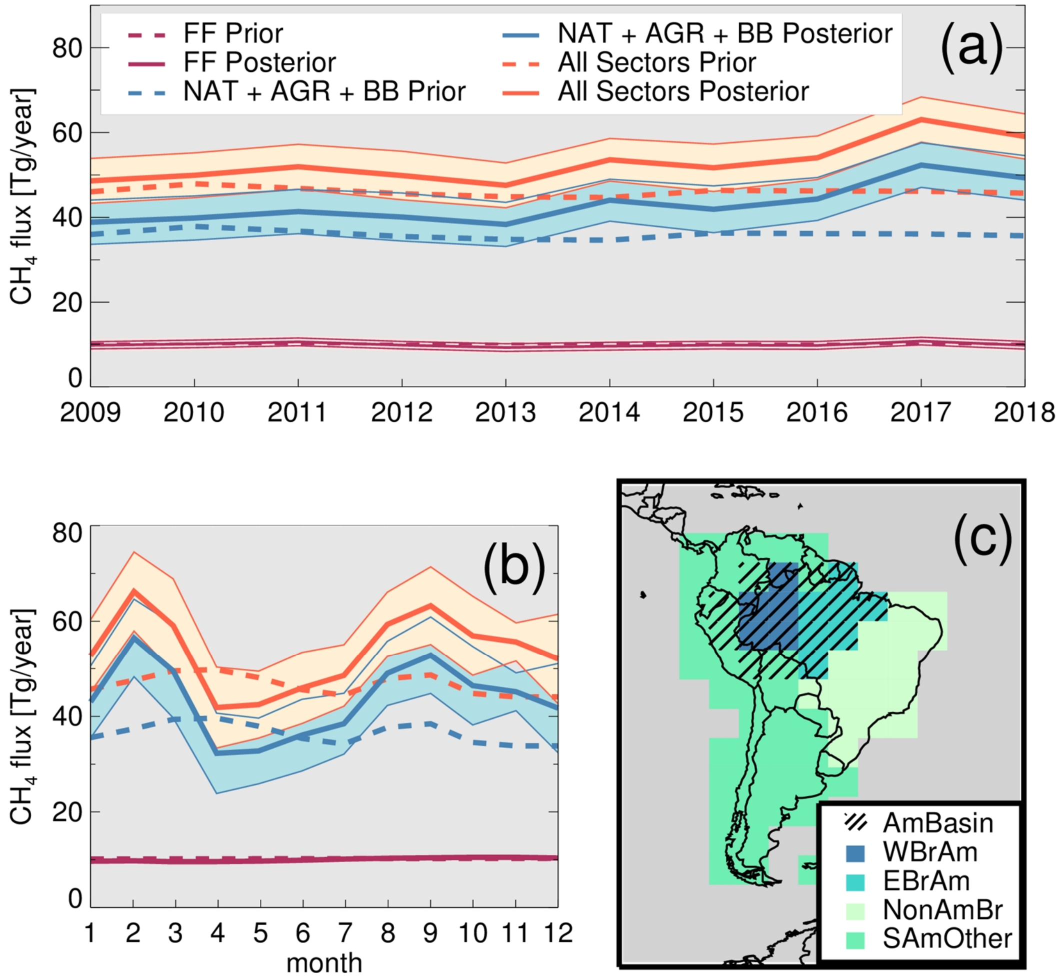

Figure 4: (a) Total annual Brazilian prior and posterior emissions (Tg(CH_4)/yr). Shaded areas show posterior uncertainties as derived in the inversion. (b) Monthly mean prior and posterior Brazilian CH4 emissions (Tg(CH_4)/yr, 2009 – 2018). Shaded areas show standard deviation for each month. (c) Regions of South America discussed in the text. Hatched area (AmBasin) represents the Amazon Basin across all countries, whilst the shaded areas show Brazilian and non-Brazilian regions.

mean flux is within the range found by Saunois et al. (2020), and agrees well with the findings of Janardanan et al. (2020). There is a significant positive trend over the whole time period (2010 – 2018) of 1.37 ± 0.69 Tg(CH_4)/yr^2 ($p < 0.05$), driven by the NAT + AGR + BB emissions category, although the distribution is more of a step-change from 2014 onwards.

Posterior emissions in Brazil peak in February and September (Figure 4b) and represent the wet-season and dry-season peaks, most likely due to contributions from the local seasonal cycles of wetland emissions and biomass burning emissions, depending on the location. The peak monthly emission rate of 66.2 ± 8.2 Tg(CH_4)/yr is in February, before lower rates of emission during the shoulder season of April to July. This February peak corresponds to a peak in precipitation across the

https://doi.org/10.5194/acp-2020-1136
Preprint. Discussion started: 10 November 2020

Atmospheric Chemistry and Physics
Discussions

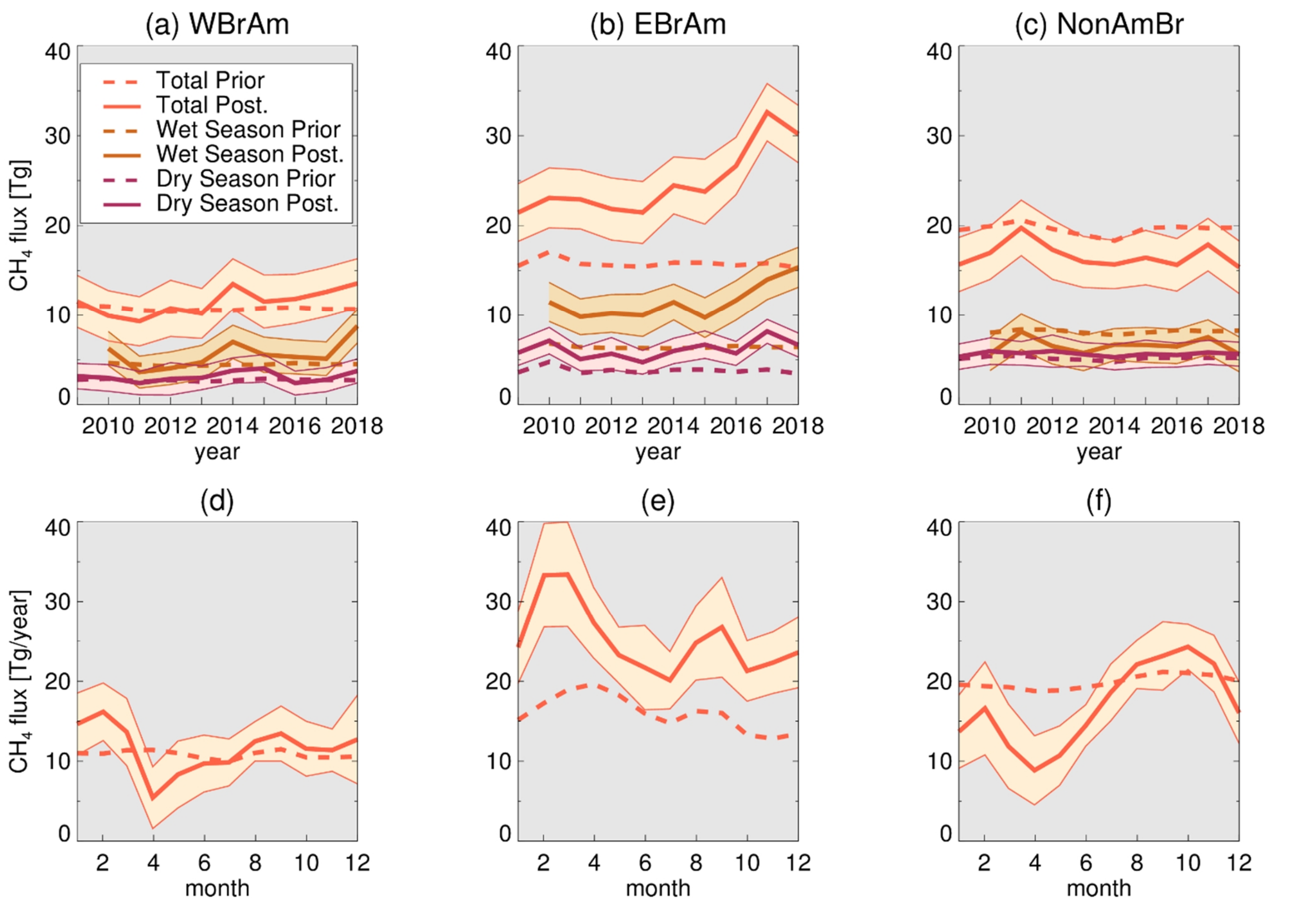

Figure 5: (a-c) Total annual (red lines) prior and posterior emissions of CH4 (Tg(CH4)/yr) in three Brazilian subregions; the western Brazilian Amazon (WBrAm), the eastern Brazilain Amazon (EBrAm) and non-Amazon Brazil (NonAmBr). Prior and posterior emissions during the wet season (December – March, brown lines) and the dry season (August – October, maroon lines) are also shown. Shading represents the posterior uncretainties for each region derived in the inversion. (d-f) Monthly mean prior and posterior emissions for the period 2009 – 2018 (Tg(CH_4)/yr) for the three sub-regions. Shading shows the standard deviation of the monthly means.

Basin (from the Global Precipitation Climatology Project (GPCP) v2.3 combined precipitation dataset (Adler et al., 2018)), but actually precedes the peak in gravity anomaly captured by the GRACE satellite (Figure S2). Emissions in August and September are almost as large as those during the peak of the wet season. Again, almost all of this seasonal variation comes from the NAT + AGR + BB emission category.

Emissions are largest in the eastern Brazilian Amazon (EBrAm, Figure 5), and are significantly larger than suggested by the prior emissions, particularly in the most recent years. The increase in emissions over the period is also largest there, rising from 22.4 ± 3.4 Tg(CH_4)/yr in 2010 – 2013 to 26.8 ± 3.3 Tg(CH_4)/yr in 2014 – 2017. Emissions also increase from 10.0 ± 2.9 Tg(CH_4)/yr to 12.3 ± 2.8 Tg(CH_4)/yr between these two periods in the western Brazilian Amazon (WBrAm). However in

https://doi.org/10.5194/acp-2020-1136
Preprint. Discussion started: 10 November 2020

Atmospheric Chemistry and Physics Discussions

the non-Amazon region of Brazil (NonAmBr), emissions decrease slightly between over these years (from 17.5 ± 3.0 Tg(CH_4)/yr to 16.4 ± 2.9 Tg(CH_4)/yr). The Amazon regions of Brazil display the two-peak seasonal cycle of CH_4 emissions, although this is much more pronounced in the east. This is most likely due to the significant effect of biomass burning within the arc of deforestation in the south-east of the Basin that usually occurs during these months. Emissions are largest in NonAmBr during the dry season, possibly due to fires in savanna regions.

We also display total emissions for each subregion during the wet season (December – March) and the dry season (August – October). These periods were defined using the GPCP precipitation data, as periods when the average monthly precipitation during 2009 – 2018 within the Basin was more than 7 mm day^{-1} and less than 3 mm day^{-1}, respectively. In both WBrAm and EBrAm, the trends for the 2009 – 2018 period are largest in the wet season. This suggests that trends in wetland emissions might be responsible for the rising CH_4 emissions.

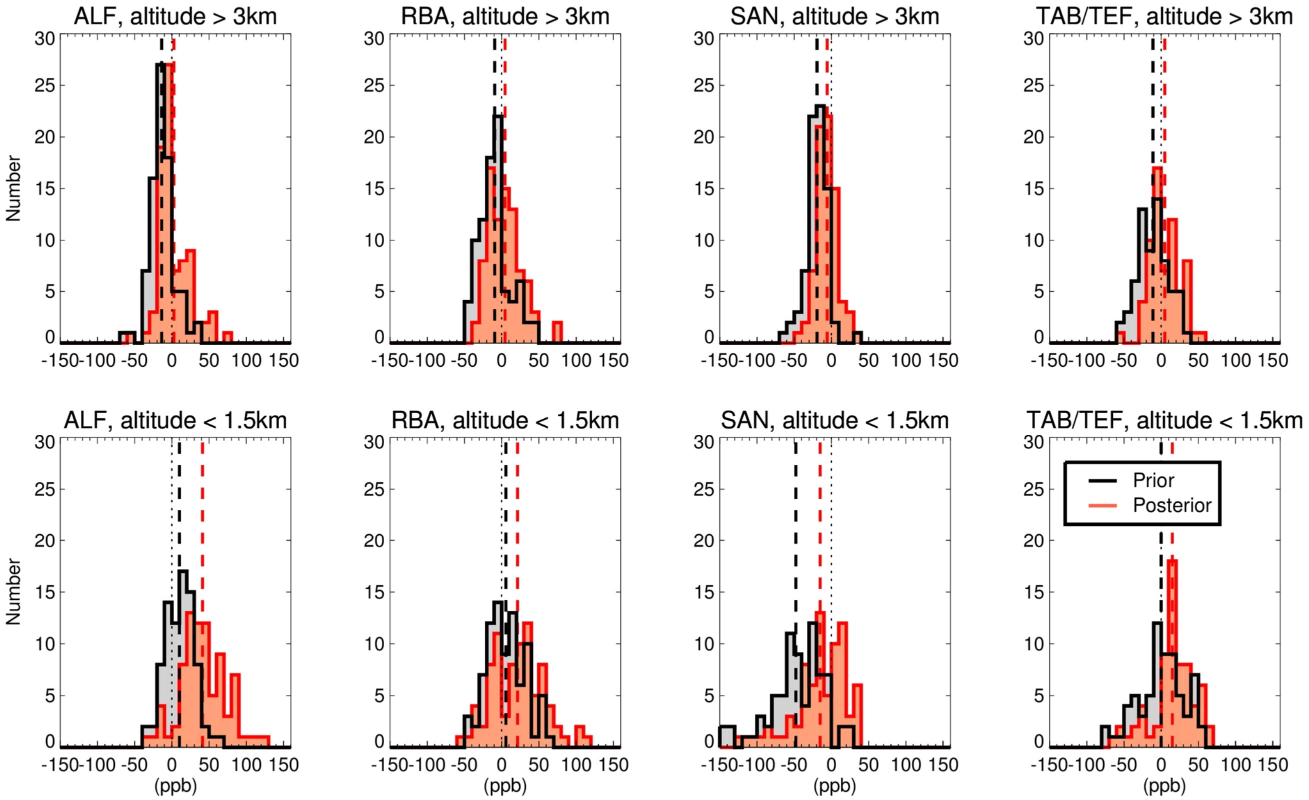

Figure 6: Histogram plots showing prior (black) and posterior (red) [model – observation] differences at the four Amazon flight locations, 2010 -2018. Measurements were taken at Alta Floresta (ALF), Rio Branco (RBA), Santarém (SAN) and Tabatinga and Tefé (TAB/TEF). Model output has been interpolated to observations locations and altitudes, before both were averaged into monthly means and into altitude bins of 3km and above (a-d) and 1.5km and below (e-h). Dotted vertical lines show the zero line, whilst dashed vertical lines show prior and posterior mean model – observation bias.

https://doi.org/10.5194/acp-2020-1136
Preprint. Discussion started: 10 November 2020

3.3 Comparison to independent observations

Observations of CH_4 made during flights within the Basin between 2010 and 2018 were used to independently check the performance of the prior and posterior emission distributions in the model (Figure 6, Table 2). For the observations made at altitudes higher than 3km, which represents the free troposphere above the Amazon, the performance of the posterior emissions is significantly improved compared to the prior at all locations. The absolute value of the model – observation bias is reduced to below 6 ppb at all sites, and the correlation between the model and the observations increases at all locations. However, the posterior performance against observations made in the boundary layer, at altitudes below 1.5 km, is generally worse than the prior performance. At the western sites, RBA and TAB/TEF, the mean bias in the model increases by approximately 15 ppb, although the correlation improves, particularly at TAB/TEF. At ALF, the correlation decreases slightly, and the mean bias increases by a large amount (31 ppb). Finally, at SAN, the performance improves significantly by both measures, with the mean bias being reduced from -47.8 ppb to -15.2 ppb. There are no significant trends in the model – aircraft residual biases in 2010 – 2017, except at TAB/TEF below 1.5km. This site has a posterior residual bias trend of +2.1 ppb/year, but this may have been caused by the change in the flight location halfway through the study period.

The improved performance at SAN is significant, as the high mole fractions of CH_4 sampled at this location relative to expectations given its location situated close to the eastern coast have been previously noted (Miller et al., 2007; Basso et al., 2016; Wilson et al., 2016). The prior model therefore leads to a large negative bias at SAN, particularly near the surface. The posterior distribution of emissions, with a region of significant emissions to the south and east of the Basin, significantly reducing the model – observation difference at SAN. The model still underestimates methane mole fractions at this site even after the improvement, however, which might still be due to remaining bias or model representation uncertainty. The fact that ALF is also located near these significant emissions leads to degradation in the model performance within the boundary layer, which was previously better at ALF than at SAN. The capability of assimilation of GOSAT XCH_4 to improve performance at both of these locations might have been reduced due to the relatively coarse model grid. Webb et al. (2016) found that comparisons between the flight-based observations and a previous version of the GOSAT XCH_4 used in this study showed that the GOSAT values were larger than equivalents estimated using the flight data at ALF, but that the discrepancy was much smaller at SAN. This being the case, it is not surprising that the model in which the GOSAT data has been assimilated has difficulties in matching the flight observations at both locations at once. Since we assimilated XCH_4 from GOSAT, which is mostly representative of the troposphere, it is expected that the model performance is improved at all locations when compared to observations made at the higher altitudes. This also indicates good model representation of inflow of CH_4 to the Basin from elsewhere. However, the fact that the posterior comparisons are generally degraded close to the surface, apart from at SAN, mean that the local sources close to these sites might be overestimated at this model resolution, that there are errors in the model's representation of vertical mixing, or that there remains a positive bias in the assimilated retrievals from GOSAT in this region. Generally, however, the temporal variation and mean bias in the model is much improved after the assimilation of GOSAT XCH_4.

https://doi.org/10.5194/acp-2020-1136
Preprint. Discussion started: 10 November 2020

Table 2: Prior and posterior bias (ppb) and correlation between TOMCAT and Amazon flight observations (2010 – 2018). Optimal values for bias and correlation for each site and altitude are highlighted in bold.

	Prior mean bias (ppb)	Posterior mean bias (ppb)	Prior correlation	Posterior correlation
ALF, >3km	-13.7	**2.6**	0.71	**0.75**
SAN, >3km	-19.4	**-5.7**	0.79	**0.88**
TAB/TEF, >3km	-11.1	**4.7**	0.67	**0.81**
RBA, >3km	-9.4	**4.6**	0.70	**0.80**
ALF, <1.5km	**10.2**	41.2	**0.70**	0.67
SAN, <1.5km	-47.8	**-15.2**	0.32	**0.49**
TAB/TEF, <1.5km	**0.0**	15.0	0.48	**0.65**
RBA, <1.5km	**5.7**	21.4	0.54	**0.56**

3.4 Bottom-up model results

The inversion suggests that CH_4 emissions have been increasing from Amazon regions throughout the 2010s, but it is not easy to determine the source sectors responsible for this rise. The largest increases over time occur during the wet season (Figure 5), when wetland emissions dominate the atmospheric signal, so it seems most likely that changes to these emissions are driving the increase. Wetland emissions are sensitive to temperature, precipitation (which drives wetland area) and carbon availability in the soil (Bloom et al., 2017), so we examined these driving factors to see how they varied during the previous decade.

The mean surface temperature within the Amazon Basin increased throughout the period 2009 - 2018 (Figure 7), while there was no significant trend in precipitation (not shown) or gravity anomaly. Estimating the trends of these factors is significantly affected by one anomalously dry and hot period, running from late 2015 to mid-2016. These record-breaking conditions were caused by the 2015/16 El Niño, and were largely confined to the east of the Basin (Jiménez-Muñoz et al., 2016). A previous extreme event during this study period, in the dry season of 2010, displayed a similar geographical distribution but was easily surpassed by the scale of the 2016 drought (Lewis et al., 2011; Jiménez-Muñoz et al., 2016). One other event that stands out is the prolonged flooded period running from though the wet season of 2013/14, during which rainfall in the south-west of the Basin was up to twice as much as usual (Espinoza et al., 2014). This flooded period did not coincide with a significant El Niño – Southern Oscillation (ENSO) period but was likely caused by warm conditions in the Subtropical South Atlantic.

Atmospheric Chemistry and Physics
Open Access
EGU
Discussions

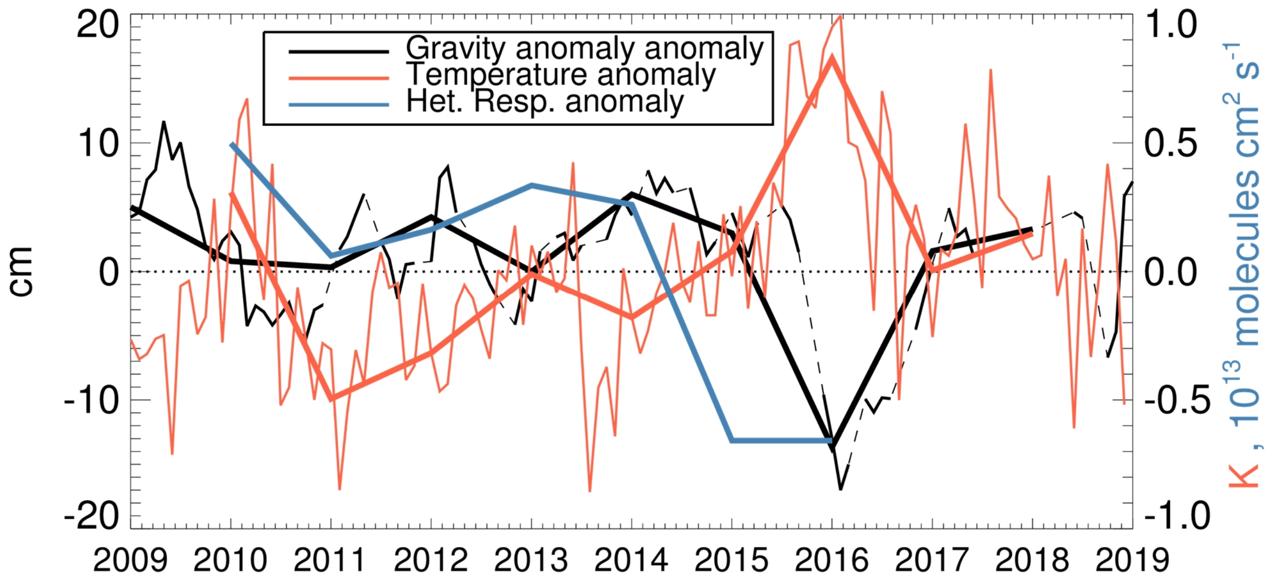

Figure 7: Anomalies of gravity anomaly (cm, black, left axis), surface temperature (K, red, right axis), and heterotrophic respiration (10^{13} molecules cm^{-2} s^{-1}, blue, right axis) for the period 2009 – 2018 within the Amazon Basin. Monthly mean anomalies are shown as thin lines, whilst wet season (December – March) averages are shown as thick lines. Interpolated values for gravity anomalies are shown as dashed lines.

We have used climate variables to examine how variations in wet season CH_4 emissions produced by the inversions might have been driven by these conditions. Figure 7 also shows the wet season mean anomalies for each year for the surface temperature, gravity anomaly and heterotrophic respiration. Wet season temperatures were high in 2010 and in 2015, 2016 and 2018. The water table was at its highest in 2012, 2014 and 2015. Finally, heterotrophic respiration was strongest in 2010, 2013 and 2014, but very low in 2015 and 2016. There was no data available for 2017, so we used a climatology value for that year. We felt that this was justified since the temperature and water table depths also had only very small anomalies during that season. As might be expected, the temperature and gravity anomalies in the wet season were strongly negatively correlated (r=-0.66), since hot and dry conditions are often linked.

The temperature trend in the Amazon was positive throughout almost the entire Basin (Figure 8a), being strongest to the far west and in the south east. The trend in the wetland fraction (Figure 8b) was more heterogeneous, with positive trends in the west contrasting with strong negative trends across the east of the Basin. For both of these variables, the trends are strongly impacted by the hot, dry conditions in the wet season of 2015/16.

The geographical distribution of the NAT + AGR + BB wet season CH_4 emission trend produced by the inversion (Figure 8c) is positive across the north west and south east of the Basin, with a fairly similar distribution to the locations with positive temperature trends. The positive emission trends in the north west are also collocated with an area with wettening trends. However, the regions to the east and south with strong positive emission trends are in the region in which wetland fraction had been decreasing as temperatures increased. This suggests that the emissions were more sensitive to the increasing temperature than to the decrease in wetland fraction or in heterotrophic respiration (not shown).

We ran the B-U model multiple times, varying the temperature response and the GRACE anomaly scaling variables within their bounds in order to produce a range of likely values for CH_4 flux from the Basin. We also used a curve fitting program in order to best reproduce the INVICAT results using the B-U model (Figures 8d and 8e). The B-U model combines the three driving variables, but the strong anti-correlation between the temperature and wetland fractions mean that this model does not produce strong variations in emissions, since the two tend to cancel out. Using the optimised B-U model produces weak positive emission trends in the west of the Basin, and weak negative trends elsewhere, giving no significant trend overall. The optimised value of q_{10} was 2.47, which is within the range of plausible values discussed in Section 2.2.3, whilst the optimised values of a_1 and a_2 were 0.73 and 0.0015, respectively. The standard deviation of the wet season emissions in the B-U model is 1.7 Tg(CH_4)/yr, compared to 2.4 Tg(CH_4)/yr in the inversion results. The mean posterior error in in the inversion results (2.9 Tg(CH_4)/yr) is relatively large compared to the standard deviation, however, meaning that the B-U model results almost always remain within the posterior inversion uncertainty. The exception to this is the wet season of 2014, when the inversion results produce larger emissions than in any other year (20.1 ± 2.7 Tg) and this feature is unable to be reproduced in the B-U model. As discussed, the wet season of 2014 was subject to extreme precipitation and widespread flooding in the Basin (Espinoza et al., 2014), and the GRACE gravity anomalies are large throughout this period (Figure 7), whilst heterotrophic respiration was high and temperatures were relatively cool (although warmer than in 2011 and 2012). Despite these conditions which seem favourable to CH_4 emission, the B-U model does not produce emissions significantly larger than any other year. The discrepancy between the inversion and B-U model results is discussed further in Section 4. We also show here the wet season emissions within the Basin from the WetCHARTS emission dataset (Bloom et al., 2017), which use a similar method to estimate wetland emissions that used in our B-U model. The values in Figure 8e are the mean values from the Full Ensemble (FE) of the WetCHARTS estimates. These emissions also show a negative trend over the period 2010 – 2017 (-0.17 Tg(CH_4)/yr), and the variation is again small (0.93 Tg(CH_4)/yr) standard deviation). They display no significant change in emissions in the wet season of 2013/14.

https://doi.org/10.5194/acp-2020-1136
Preprint. Discussion started: 10 November 2020

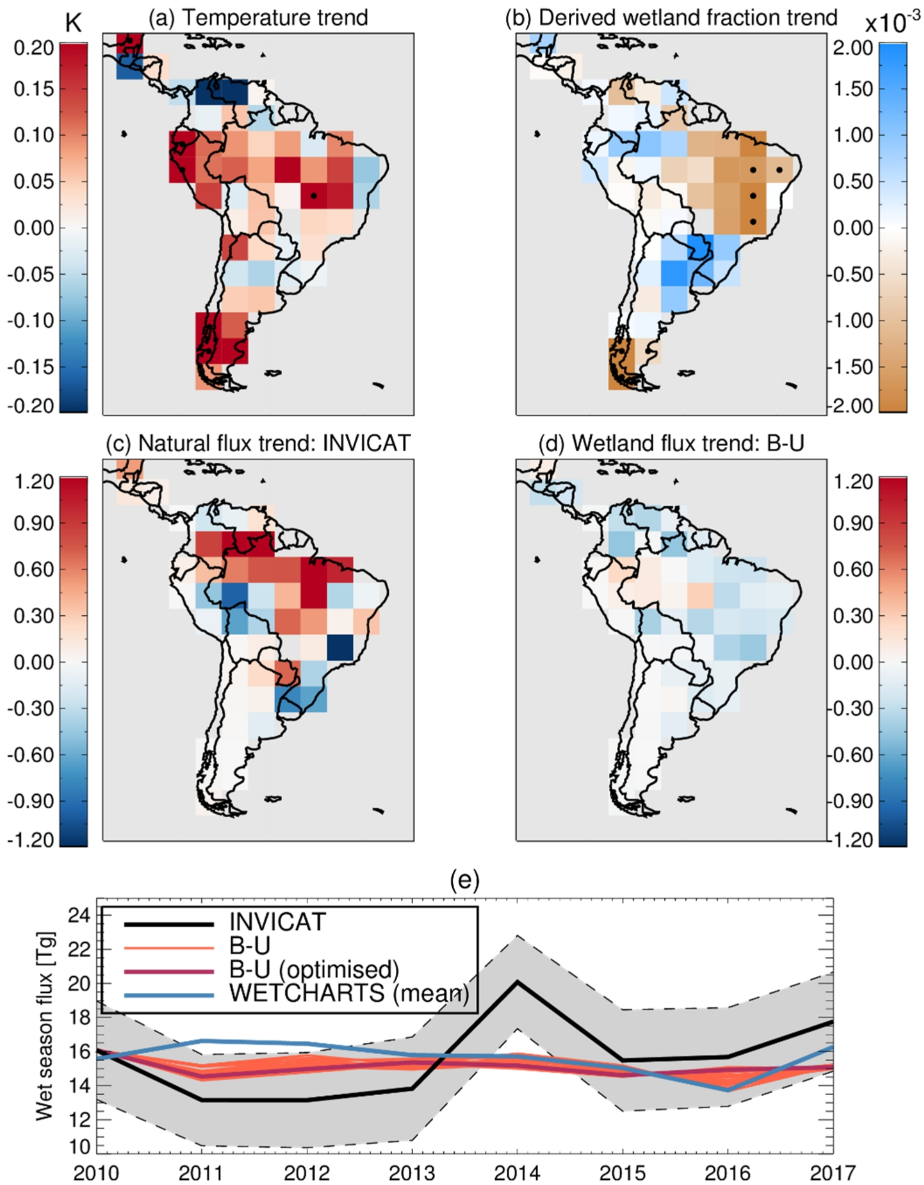

Figure 8: Average wet season trends for the period 2010 – 2017 for (a) temperature in K year^{-1}; (b) wetland fraction grid cell^{-1} year^{-1}; (c) NAT + AGR + BB CH_4 surface flux in mg m^{-2} day^{-1} year^{-1} from GOSAT inversion; and (d) Optimised bottom-up (B-U) model surface flux of CH_4 in mg m^{-2} day^{-1} year^{-1}. (e) Total Amazon Basin wet season CH_4 emissions in Tg (2010 – 2017) from GOSAT inversion (black line, with grey shading representing posterior uncertainty). Red lines show ensemble of B-U model simulations, and maroon line is the optimised B-U model. Blue line shows the mean of the WetCHARTS Full Ensemble wet season flux.

https://doi.org/10.5194/acp-2020-1136
Preprint. Discussion started: 10 November 2020

Atmospheric Chemistry and Physics Discussions

4 Discussion

We derive emissions of CH_4 in Brazil for the period 2010 – 2018 of 52.7 ± 5.3 Tg(CH_4)/yr, split into two periods during which mean Brazilian emissions were 49.8 ± 5.4 in 2010 – 2013 and 55.6 ± 5.2 in 2014 – 2017, an increase of 5.8 ± 5.2 Tg(CH_4)/yr. This increase was found to be entirely due to the NAT + AGR + BB emissions within the Amazon region.

This increase between the two periods is very similar to that found by Tunnicliffe et al., (2020), although the total emissions found in our study are larger than their finding of 33.3 ± 3.7 Tg(CH_4)/yr. They removed a model – satellite bias of 22 ± 8 ppb from the GOSAT observations used in their study, which is much larger than our bias of 3 – 9 ppb removed from XCH_4 over the Amazon. This larger bias removal, coupled with the different model transport of their regional inversion, could explain the smaller emissions that they derive. The positive biases in our posterior CH_4 relative to aircraft observations within the boundary layer also suggests that our emissions may be overestimated. However, we note the absence of significant trends in posterior model minus aircraft residuals between 2010 – 2017. Our posterior total emissions agree well with the findings of Janardanan et al., (2020), however, who derived Brazilian emissions of 56.2 ± 10 Tg(CH_4)/yr for the period 2011 – 2017, although any change in this value over time was not discussed in that study. Yin et al., (2020) did not report total emissions, but found a rise in Amazonian emissions of 4.2 ± 1.2 Tg(CH_4)/yr over 2010 – 2017, along with small increases in eastern Brazil. A group of 22 inverse model experiments presented by Saunois et al., (2020) produced a range of 47.3 – 78.2 Tg(CH_4)/yr for Brazilian emissions during the 2008 – 2017 period, although one of these results used the TOMCAT forward model to represent the atmospheric transport, so is not fully independent from our results. Our findings here are within the range of these models, albeit towards the lower end. The majority of these top-down studies used either the same GOSAT and surface observation data used in our study, or some variation of it. The fact that the derived emissions using similar observation data can vary so much highlights the inherent uncertainties still remaining in top-down studies of CH_4 emissions, with differences in model transport, chemistry representation, inversion methodology, bias correction and error assumptions all contributing to differences in results.

The increase in emissions from 2014 onwards that we derive coincides with a faster rate of increase in the observed surface mole fraction of CH_4 (Nisbet et al., 2019). Unfortunately, the extent that the increase in observed mole fractions in the atmosphere is driven by increasing Amazon emissions is difficult to constrain without more extensive knowledge of the atmospheric chemical loss of CH_4. Our global inversion, using repeating OH values each year, indicates that the increase of 5.8 ± 5.2 Tg(CH_4)/yr from Amazon emissions is responsible for 24 ± 18% of the global total increase in emissions between 2010-13 and 2014-17, which was 24.1 ± 15.0 Tg(CH_4)/yr.

The Amazon emissions derived in this study for 2010 and 2011 (41.6 ± 5.3 Tg(CH_4)/yr) are a little above the higher limit of those found in our previous study using the flight observations only (31.6 – 41.1 Tg(CH_4)/yr, Wilson et al., (2016)). This

https://doi.org/10.5194/acp-2020-1136
Preprint. Discussion started: 10 November 2020

indicates that using the vertical profile data only to calculate Basin-wide emission totals may lead to a small underestimation of the total compared to using satellite data. This discrepancy is supported by the positive bias seen in this study within the boundary layer at most of the sites when comparing the posterior model output to the in situ flight observations. However, the emission totals are fairly similar across the different methodologies, with the caveat that the same transport model was used for both findings.

Our comparisons to the independent observations taken during flights within the Amazon highlight both some success and some remaining issues with our results. Assimilating the GOSAT data leads to an improvement compared to the prior in the mean bias and correlation at all four locations when observations made above the boundary layer are considered. However, the posterior comparison to observations made close to the surface are inferior to the prior comparison at three of the locations. It seems that improving the performance compared to the GOSAT data throughout the troposphere is at the expense of reducing performance at the surface. There could, therefore, be transport errors in the inverse model, possibly in the boundary layer transport. It is possible also that the relatively coarse resolution of the inversion leads to poorer comparisons to the boundary layer observation. Finally, as stated by Webb et al. (2016), comparisons between the flight observations and GOSAT at the Alta Floresta (ALF) site, which displays the worst posterior performance in the model, are also not as good as at other locations. Despite the increased posterior bias in the boundary layer at three of the sites, the improved performance at Santarém suggests that the significant emissions close to the mouth of the Amazon derived by the inversion are potentially a realistic feature, consistent with the previous in situ data-based flux estimates of Miller et al. (2007) and Basso et al. (2016). However, the degradation in performance at Alta Floresta, also in the east of the Basin, suggests that the strong emissions do not extend as far south as in our model posterior. We will in the future produce inversions at higher resolution to investigate this feature further.

Due to computational constraints, we could not carry out inversions for the entire GOSAT period using a higher horizontal resolution than the one chosen for our inverse model, but to examine the sensitivity of our results to the model resolution, we ran an inversion for 2010 at 2.8° horizontal grid resolution (Figure S3), averaging the GOSAT XCH_4 onto this model grid. We did not split the results into different source sectors, instead deriving total CH_4 surface flux. Otherwise the model set-up was identical to the 5.6° inversions of the main study. Many of the features of the posterior solution are identical to those of the coarser grid, with higher emissions from the region to the south and east of the Amazon river, and a decrease in emissions from the south of Brazil, near the densely populated cities. However, there is no decrease in emissions to the west of the Amazon Basin, as consistently seen when using the coarser model grid. Total derived emissions for Brazil and for the Amazon Basin are similar when using the 2.8° and the 5.6° grids, however. We derive total posterior emissions for Brazil in 2010 of 49.9 Tg(CH_4)/yr using the coarser grid, and 51.4 Tg(CH_4)/yr using the finer grid.

Our derived positive trends are largest during the wet season within the east Amazon, indicating that increasing flux from wetland sources are most likely responsible for the increase in total emissions. However, attempting to reproduce these trends, and the interannual variations, using a B-U model was largely unsuccessful. Although the B-U model mainly stayed within the uncertainty derived in the inversion, it was unable to capture a large increase in emissions in the wet season of 2014. This indicates either that the variation produced in INVICAT was exaggerated, that uncertainty in the B-U model set-up and input data led to this inability to match the inversion results, or some combination of these factors. It is also possible that biomass burning CH_4 flux has increased in the region outside of the dry season (e.g. Silva Junior et al. (2019)), which would not be captured in our B-U model.

Potential errors within the inverse model are likely due to one of five factors. The model transport, repeating OH, error covariance matrices, satellite retrieval uncertainty and method of comparing the model and satellite can all affect the posterior results. Regarding the use of repeating OH values for each year of the inversion, however, it should be noted that Tunnicliffe et al., (2020) used a regional model in which the chemical sink of CH_4 was not a factor, and found similar levels of interannual variably to those produced here.

Meanwhile, our B-U model was much simpler than full land surface models and used only one input source for each set driving of data. The fact that wetland fraction and temperature were strongly anti-correlated meant that the model was not able to produce significant emission variations from year to year when the two were included in the model. In the future we plan to use a more complex land surface model for comparisons such as this, but our use of the JULES model to produce our prior emissions inventory meant that it would have been inappropriate for post hoc comparisons here. The independent WetCHARTS results, however, also produced very different results to those of our inversion.

The performance of the B-U model compared to the inverse model suggests conflicting hypotheses. The positive trend in emissions produced in INIVCAT was concurrent with increasing temperatures across much of the Amazon. This indicates that the temperature response of wetland emissions in the region might be high. However, the fact that the B-U model was unable to produce significantly larger emissions during the 2014 wet season, as were produced by the inversion, despite large wetland fraction and heterotrophic respiration at the time, indicates that the wetland fraction response might also be high, and potentially non-linear. Comparing the results from the B-U model for 2012 and 2014 is instructive, as 2014 had higher heterotrophic respiration and temperature, and a similar (but slightly higher) mean wetland fraction. However, the B-U emission totals for these two years were very similar. Although the observed mean gravity anomalies were similar, they were characterised differently, with prolonged positive anomalies throughout 2013/14, but a short and intense positive anomaly during the end of the 2012 wet season. This suggests that emissions could be a function of the period of time for which the soil is saturated. It should be noted that Tunnicliffe et al. (2020) also derived large CH_4 fluxes during this wet season, but they were allocated to anthropogenic sources rather than wetlands using their methodology, likely due to differences in the transport model and sector allocation method. Increased complexity in the B-U model and examination of correlations between inversely-derived fluxes and potential wetland flux drivers are both necessary for future comparisons, and for now it is not possible to determine definitively the cause of the trend in CH_4 emissions in the Amazon Basin.

5 Conclusions

Our global inversion of CH_4 emissions using satellite data and surface observations allowed us to quantify changes in South American emissions over the period 2009 – 2018. We found that emissions increased during this period, particularly during the wet season of December - March. Total Brazilian emissions rose from 49.8 ± 5.4 Tg(CH_4)/yr in 2010 – 2013 to 55.6 ± 5.2 Tg(CH_4)/yr in 2014 – 2017, whilst natural emissions from the Amazon Basin (from all countries)), an area of 6.9 million km^2 on this model grid, rose from 38.2 ± 5.3 Tg(CH_4)/yr to 45.6 ± 5.2 Tg(CH_4)/yr. We show that there was significant emission from the south and east of the Basin throughout this period, and that the positive trends were largest in the east Brazilian Amazon. We derive particularly large emissions during the 2013/14 wet season, a period during which there were widespread flooding. It is significant that our inversions show improved performance at Santarém due to the large emissions in the east of the Basin, similar to previous aircraft-based studies (Miller et al., 2007; Basso et al., 2016). Indeed, based on the remaining negative model-observation bias at that location, it is possible that CH_4 emissions affecting that location could be even larger. However, it appears that the Alta Floresta site is overly affected by these large emissions in our analysis, indicating that the southerly extent of the large emissions might be too great.

However, attempting to reproduce these trends in a simple bottom-up model were unsuccessful, mainly due to strong anti-correlations between the wetland fraction and the temperature within the Basin leading to little variation in annual wet season emissions. This suggests that the complexity of the model must be increased in order to fully represent the relationship between carbon availability, wetland fraction and soil temperature. Our B-U model, and other models (Bloom et al., 2017), suggest a negative trend in emissions from driving conditions, but this is at odds with our findings and those of others. This suggests that temperature has a strong role to play in wetland emissions of CH_4 in the Amazon region, since this has also had an increasing trend over the past decade. It is also important to consider the role of wetland variability, however. For the inverse model the contribution of how sinks of CH_4 in the atmosphere might have varied should also be considered.

The results of our inversion are in agreement with previous studies (e.g. Janardanan et al., (2020)), and within the range provided by Saunois et al. (2020). However, our posterior emissions from Brazil are significantly larger than those produced by Tunnicliffe et al. (2020) using a similar observational data set, showing the importance of model transport in inversion results.

https://doi.org/10.5194/acp-2020-1136
Preprint. Discussion started: 10 November 2020

Atmospheric Chemistry and Physics Discussions

Our results show that the Amazon Basin was responsible for 24 ± 18% of the total global increase in CH_4 emissions during the last decade, and it could contribute further in future due to its sensitivity to increasing temperature. Our study shows the benefit of using satellite data to inform on emissions of CH_4, particularly in poorly sampled tropical regions, along with the benefits of long-term satellite missions to produce large-scale, consistent datasets. As the satellites and models improve, we can further refine our estimates of emissions from the important and changing role of South American ecosystems on global methane variability.

Appendix A

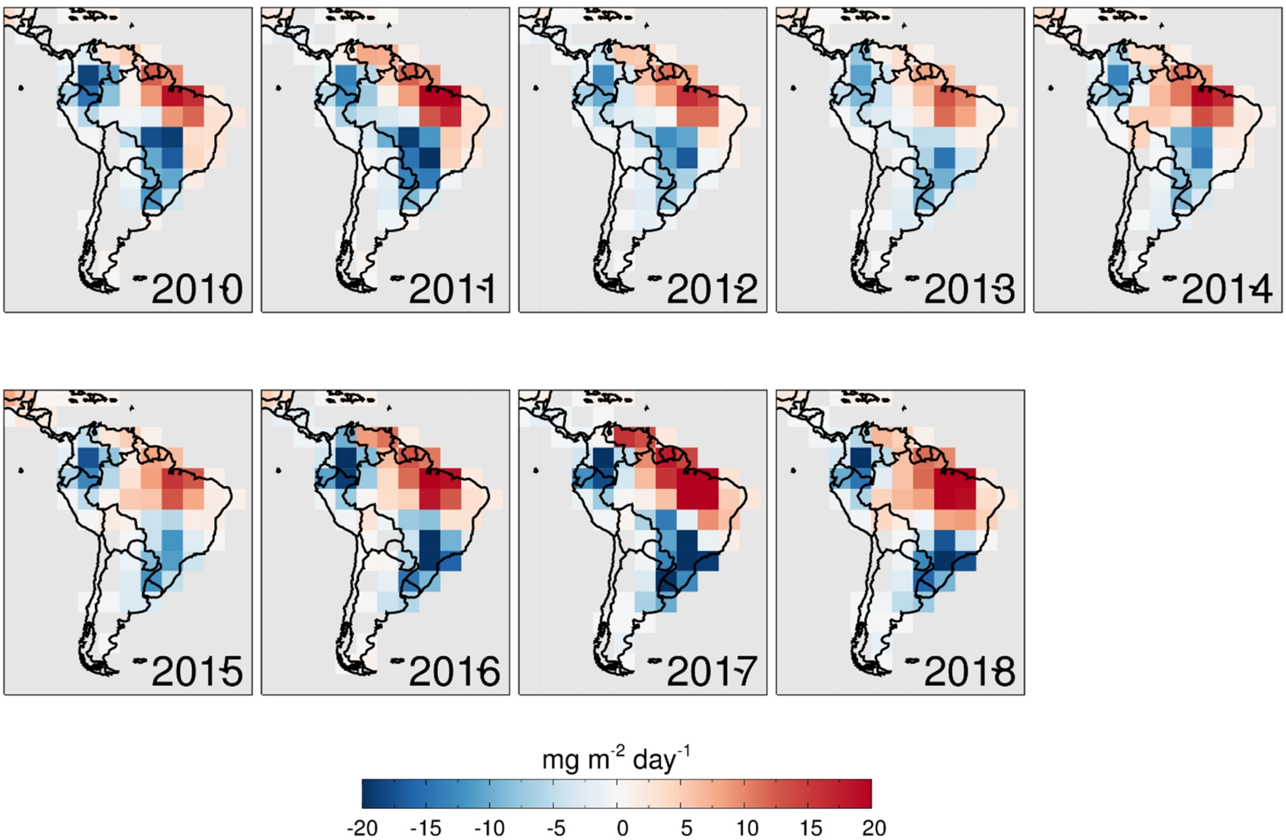

Figure A1: Annual mean (posterior – prior) gridded total South American CH_4 emissions (mg m^{-2} day^{-1}) for each year covering the period 2010 – 2018.

https://doi.org/10.5194/acp-2020-1136
Preprint. Discussion started: 10 November 2020

Atmospheric Chemistry and Physics Discussions

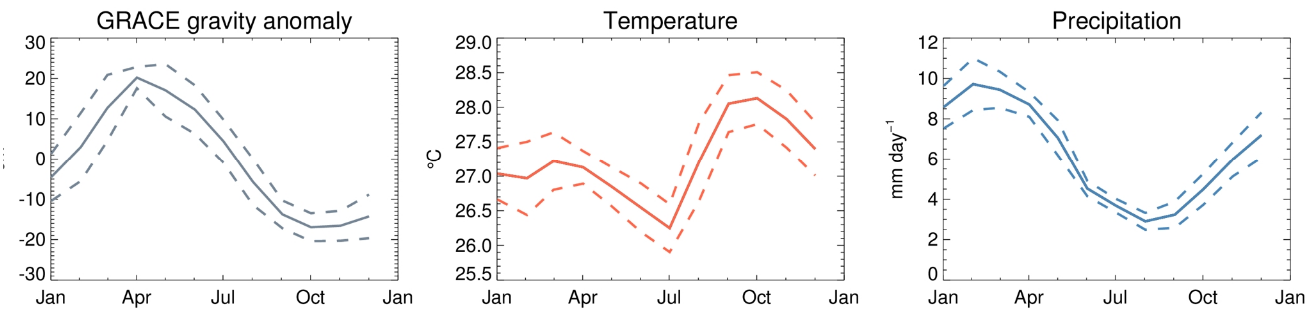

Figure A2: Mean seasonal cycle of GRACE gravity anomaly (left, cm), temperature (centre, °C) and precipitation (right, mm day^{-1}) within the Amazon Basin for 2010 – 2018. Dashed lines show one standard deviation from the mean values. Temperature is taken from the NOAA/NCEP Global Historical Climatology Network v2 and the Climate Anomaly Monitoring System GHCN Gridded v2, whilst precipitation is from the Global Precipitation Climatology Project v2.3 combined precipitation dataset.

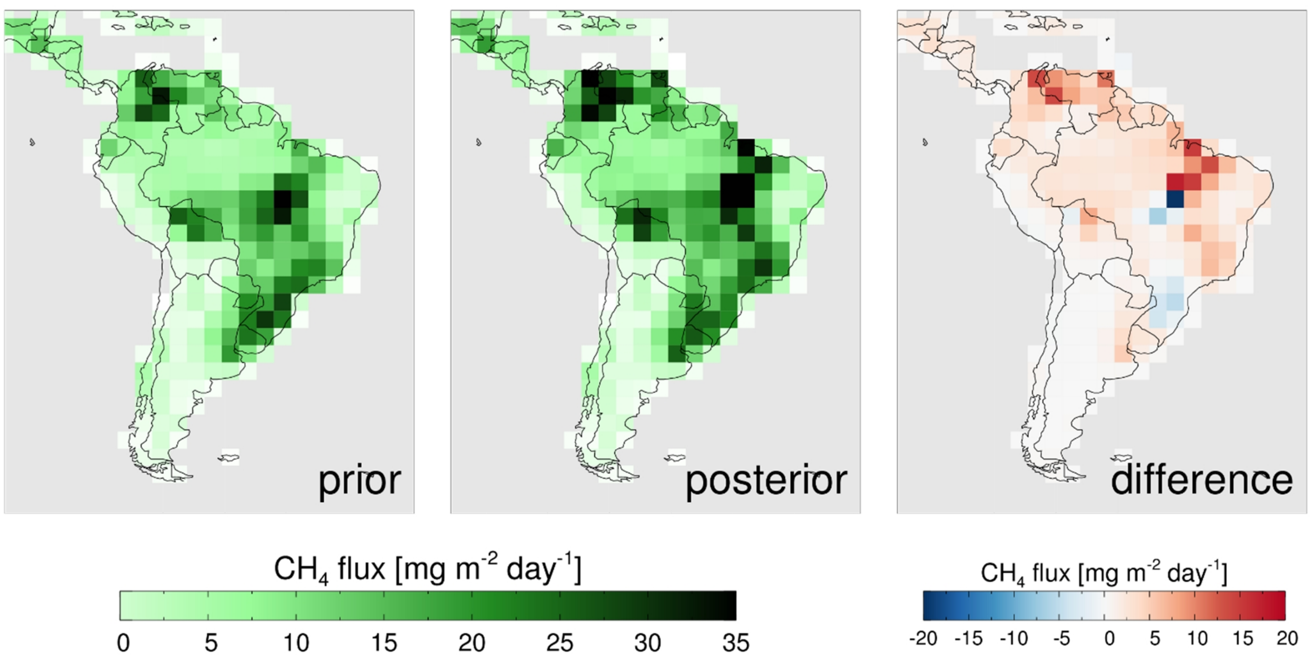

Figure A3: Prior (left) and posterior (centre) emissions of CH_4 (mg m^{-2} day^{-1}) for 2010 from an inversion carried out on the 2.8° degree model grid. (Right) Posterior – prior emissions.

https://doi.org/10.5194/acp-2020-1136
Preprint. Discussion started: 10 November 2020

Table A4: Locations and time periods covered by surface flask samples used in inversions, provided by the National Oceanic and Atmospheric Administration's Global Monitoring Laboratory.

Station code	Longitude, Latitude (°)	Time Period	Station code	Longitude, Latitude (°)	Time Period
`ABP	321.8E, 12.8S	2009 – 2010	LLN	120.9E, 23.5N	2009 – 2018
ALT	297.5E, 82.5N	2009 – 2018	LMP	12.6E, 35.5N	2009 – 2018
AMY	126.3E, 36.5N	2013 – 2018	MEX	262.7E, 19.0N	2009 – 2018
ASC	345.6E, 8.0S	2009 – 2018	MHD	350.1E, 53.3N	2009 – 2018
ASK	5.6E, 23.3N	2009 – 2018	MID	182.6E, 28.2N	2009 – 2018
AZR	332.6E, 38.8N	2009 – 2018	MKN	37.3E, 0.0S	2009 – 2011
BAL	17.0E, 55.4N	2009 – 2011	MLO	204.4E, 19.5N	2009 – 2018
BHD	174.9E, 41.4S	2009 – 2018	NAT	324.8E, 5.8S	2010 – 2018
BKT	100.3E, 0.2S	2009 – 2018	NMB	15.0E, 23.6S	2009 – 2018
BME	295.3E, 32.4N	2009 – 2010	NWR	254.4, 40.0N	2009 – 2018
BMW	295.1E, 32.3N	2009 – 2018	OXK	11.8E, 50.0N	2009 – 2018
BRW	203.4E, 71.3N	2009 – 2018	PAL	24.1E, 68.0N	2009 – 2018
BSC	28.7E, 44.2N	2009 – 2011	PSA	296.0E, 65.0S	2009 – 2018
CBA	197.3E, 55.2N	2009 – 2018	PTA	236.3E, 39.0N	2009 – 2011
CGO	144.7E, 55.2N	2009 – 2018	RPB	300.6E, 13.2N	2009 – 2018
CHR	202.8E, 1.7N	2009 – 2018	SDZ	117.1E, 40.7N	2009 – 2015
CIB	355.1E, 41.8N	2009 – 2018	SEY	55.5E, 4.7S	2009 – 2018
CPT	18.5E, 34.4S	2010 – 2018	SHM	174.1E, 52.7N	2009 – 2018
CRZ	51.9E, 46.4S	2009 – 2018	SMO	189.4E, 14.3S	2009 – 2018
DRP	296.3E, 59.0S	2009 – 2018	STM	2.0E, 66.0N	2009
DSI	116.7E, 20.7N	2010 – 2018	SUM	321.6E, 72.6N	2009 – 2018
EIC	250.5E, 27.2S	2009 – 2018	SYO	39.6E, 69.0S	2009 – 2018
GMI	144.7E, 13.4N	2009 – 2018	TAC	1.1E, 52.5N	2014 – 2015
HBA	333.8E, 75.6S	2009 – 2018	TAP	126.1E, 36.7N	2009 – 2018
HPB	11.0E, 47.8N	2009 – 2018	THD	235.8E, 41.1N	2009 – 2017
HSU	235.3E, 41.0N	2009 – 2017	TIK	128.9E, 71.6N	2011 – 2018
HUN	16.7E, 47.0N	2009 – 2018	USH	291.7E, 54.9S	2009 – 2018
ICE	339.7E, 63.4N	2009 – 2018	UTA	246.3E, 39.9N	2009 – 2018
IZO	343.5E, 28.3N	2009 – 2018	UUM	111.1E, 44.5N	2009 – 2018
KEY	279.8E, 25.7N	2009 – 2018	WIS	35.1E, 30.0N	2009 – 2018
KUM	205.0E, 19.7N	2009 – 2018	WLG	100.9E, 36.3N	2009 – 2018
KZD	76.9E, 44.1N	2009	ZEP	11.9E, 78.9N	2009 – 2018
KZM	77.9E, 43.2N	2009			

Author contributions. C.W., M.P.C. and M.G. designed the methodology and wrote the manuscript. C.W. performed the analysis. R.J.P and H.B. provided the GOSAT data. J.M. and S.A.M. provided TOMCAT model input. L.V.G., J.B.M. and L.S.B provided the Amazon flight data. All authors contributed with analysis and text.

Code and data availability. University of Leicester GOSAT Proxy XCH_4 data can be accessed via the Copernicus Climate Data Store or by contacting Rob Parker. The forward and inverse TOMCAT output used in this study can be accessed by contacting Chris Wilson and Martyn Chipperfield.

Competing interests. We declare no conflicts of interest.

Acknowledgements

CW, MPC, RJP and HB are funded via the UK National Centre for Earth Observation (NE/R016518/1 and NE/N018079/1). We thank the Japanese Aerospace Exploration Agency, National Institute for Environmental Studies, and the Ministry of Environment for the GOSAT data and their continuous support as part of the Joint Research Agreement. This research used the ALICE High Performance Computing Facility at the University of Leicester for the GOSAT retrievals. LVG, LSB, JBM are funded via the following grants: FAPESP (16/02018-2, 11/51841-0, 08/58120-3, 18/14006-4), NASA grants (11-CMS11-0025, NRMJ1000-17-00431), ERC Horizon 2020 (649087) and 7FP EU (283080).

References

Adler, R.F., Sapiano, M.R.P., Huffman, G.J., Wang, J.-J., Gu, G., Bolvin, D., Chiu, L., Schneider, U., Becker, A., Nelkin, E., Xie, P., Ferraro, R., Shin, D.-B., 2018. The Global Precipitation Climatology Project (GPCP) Monthly Analysis (New Version 2.3) and a Review of 2017 Global Precipitation. Atmosphere 9, 138. https://doi.org/10.3390/atmos9040138

Basso, L.S., Gatti, L.V., Gloor, M., Miller, J.B., Domingues, L.G., Correia, C.S.C., Borges, V.F., 2016. Seasonality and interannual variability of CH4 fluxes from the eastern Amazon Basin inferred from atmospheric mole fraction profiles. Journal of Geophysical Research: Atmospheres 121, 168–184. https://doi.org/10.1002/2015JD023874

Bloom, A.A., Bowman, K.W., Lee, M., Turner, A.J., Schroeder, R., Worden, J.R., Weidner, R., McDonald, K.C., Jacob, D.J., 2017. A global wetland methane emissions and uncertainty dataset for atmospheric chemical transport models (WetCHARTs version 1.0). Geoscientific Model Development 10, 2141–2156. https://doi.org/10.5194/gmd-10-2141-2017

Bloom, A.A., Palmer, P.I., Fraser, A., Reay, D.S., Frankenberg, C., 2010. Large-Scale Controls of Methanogenesis Inferred from Methane and Gravity Spaceborne Data. Science 327, 322–325. https://doi.org/10.1126/science.1175176

Bousserez, N., Henze, D.K., Perkins, A., Bowman, K.W., Lee, M., Liu, J., Deng, F., Jones, D.B.A., 2015. Improved analysis-error covariance matrix for high-dimensional variational inversions: application to source estimation using a 3D atmospheric transport model. Quarterly Journal of the Royal Meteorological Society 141, 1906–1921. https://doi.org/10.1002/qj.2495

Chevallier, F., 2007. Impact of correlated observation errors on inverted CO2 surface fluxes from OCO measurements. Geophysical Research Letters 34. https://doi.org/10.1029/2007GL030463

Chipperfield, M.P., 2006. New version of the TOMCAT/SLIMCAT off-line chemical transport model: Intercomparison of stratospheric tracer experiments. Quarterly Journal of the Royal Meteorological Society 132, 1179–1203. https://doi.org/10.1256/qj.05.51

https://doi.org/10.5194/acp-2020-1136
Preprint. Discussion started: 10 November 2020

Clark, D.B., Mercado, L.M., Sitch, S., Jones, C.D., Gedney, N., Best, M.J., Pryor, M., Rooney, G.G., Essery, R.L.H., Blyth, E., Boucher, O., Harding, R.J., Huntingford, C., Cox, P.M., 2011. The Joint UK Land Environment Simulator (JULES), model description – Part 2: Carbon fluxes and vegetation dynamics. Geoscientific Model Development 4, 701–722. https://doi.org/10.5194/gmd-4-701-2011

Dee, D.P., Uppala, S.M., Simmons, A.J., Berrisford, P., Poli, P., Kobayashi, S., Andrae, U., Balmaseda, M.A., Balsamo, G., Bauer, P., Bechtold, P., Beljaars, A.C.M., Berg, L. van de, Bidlot, J., Bormann, N., Delsol, C., Dragani, R., Fuentes, M., Geer, A.J., Haimberger, L., Healy, S.B., Hersbach, H., Hólm, E.V., Isaksen, L., Kållberg, P., Köhler, M., Matricardi, M., McNally, A.P., Monge-Sanz, B.M., Morcrette, J.-J., Park, B.-K., Peubey, C., Rosnay, P. de, Tavolato, C., Thépaut, J.-N., Vitart, F., 2011. The ERA-Interim reanalysis: configuration and performance of the data assimilation system. Quarterly Journal of the Royal Meteorological Society 137, 553–597. https://doi.org/10.1002/qj.828

Dlugokencky, E.J., Lang, P.M., Crotwell, A.M., Mund, J.W., Crotwell, M.J., Thoning, K.W., 2018. Atmospheric Methane Dry Air Mole Fractions from the NOAA ESRL Carbon Cycle Cooperative Global Air Sampling Network, 1983-2017. Version: 2018-08-01 ftp://aftp.cmdl.noaa.gov/data/trace_gases/ch4/flask/surface/.

do Carmo, J.B., Keller, M., Dias, J.D., Camargo, P.B. de, Crill, P., 2006. A source of methane from upland forests in the Brazilian Amazon. Geophysical Research Letters 33. https://doi.org/10.1029/2005GL025436

Espinoza, J.C., Marengo, J.A., Ronchail, J., Carpio, J.M., Flores, L.N., Guyot, J.L., 2014. The extreme 2014 flood in south-western Amazon basin: the role of tropical-subtropical South Atlantic SST gradient. Environ. Res. Lett. 9, 124007. https://doi.org/10.1088/1748-9326/9/12/124007

Fan, Y., Dool, H. van den, 2008. A global monthly land surface air temperature analysis for 1948–present. Journal of Geophysical Research: Atmospheres 113. https://doi.org/10.1029/2007JD008470

Feng, L., Palmer, P.I., Bösch, H., Parker, R.J., Webb, A.J., Correia, C.S.C., Deutscher, N.M., Domingues, L.G., Feist, D.G., Gatti, L.V., Gloor, E., Hase, F., Kivi, R., Liu, Y., Miller, J.B., Morino, I., Sussmann, R., Strong, K., Uchino, O., Wang, J., Zahn, A., 2017. Consistent regional fluxes of CH_4 and CO_2 inferred from GOSAT proxy $XCH_4 : XCO_2$ retrievals, 2010–2014. Atmospheric Chemistry and Physics 17, 4781–4797. https://doi.org/10.5194/acp-17-4781-2017

Fraser, A., Palmer, P.I., Feng, L., Boesch, H., Cogan, A., Parker, R., Dlugokencky, E.J., Fraser, P.J., Krummel, P.B., Langenfelds, R.L., O'Doherty, S., Prinn, R.G., Steele, L.P., van der Schoot, M., Weiss, R.F., 2013. Estimating regional methane surface fluxes: the relative importance of surface and GOSAT mole fraction measurements. Atmospheric Chemistry and Physics 13, 5697–5713. https://doi.org/10.5194/acp-13-5697-2013

Fujita, R., Morimoto, S., Maksyutov, S., Kim, H.-S., Arshinov, M., Brailsford, G., Aoki, S., Nakazawa, T., 2020. Global and Regional CH4 Emissions for 1995–2013 Derived From Atmospheric CH4, δ13C-CH4, and δD-CH4 Observations and a Chemical Transport Model. Journal of Geophysical Research: Atmospheres 125, e2020JD032903. https://doi.org/10.1029/2020JD032903

Gatti, L.V., Gloor, M., Miller, J.B., Doughty, C.E., Malhi, Y., Domingues, L.G., Basso, L.S., Martinewski, A., Correia, C.S.C., Borges, V.F., Freitas, S., Braz, R., Anderson, L.O., Rocha, H., Grace, J., Phillips, O.L., Lloyd, J., 2014. Drought sensitivity of Amazonian carbon balance revealed by atmospheric measurements. Nature 506, 76–80. https://doi.org/10.1038/nature12957

Gloor, E., Wilson, C., Chipperfield, M.P., Chevallier, F., Buermann, W., Boesch, H., Parker, R., Somkuti, P., Gatti, L.V., Correia, C., Domingues, L.G., Peters, W., Miller, J., Deeter, M.N., Sullivan, M.J.P., 2018. Tropical land carbon cycle responses to 2015/16 El Niño as recorded by atmospheric greenhouse gas and remote sensing data. Philosophical Transactions of the Royal Society B: Biological Sciences 373, 20170302. https://doi.org/10.1098/rstb.2017.0302

Gumbricht, T., Roman-Cuesta, R.M., Verchot, L., Herold, M., Wittmann, F., Householder, E., Herold, N., Murdiyarso, D., 2017. An expert system model for mapping tropical wetlands and peatlands reveals South America as the largest contributor. Global Change Biology 23, 3581–3599. https://doi.org/10.1111/gcb.13689

Howarth, R.W., 2019. Ideas and perspectives: is shale gas a major driver of recent increase in global atmospheric methane? Biogeosciences 16, 3033–3046. https://doi.org/10.5194/bg-16-3033-2019

Huijnen, V., Williams, J., Weele, M. van, Noije, T. van, Krol, M., Dentener, F., Segers, A., Houweling, S., Peters, W., Laat, J. de, Boersma, F., Bergamaschi, P., Velthoven, P. van, Sager, P.L., Eskes, H., Alkemade, F., Scheele, R., Nédélec, P., Pätz, H.-W., 2010. The global chemistry transport model TM5: description and evaluation of the tropospheric chemistry version 3.0. Geoscientific Model Development 3, 445–473. https://doi.org/10.5194/gmd-3-445-2010

Jackson, R.B., Saunois, M., Bousquet, P., Canadell, J.G., Poulter, B., Stavert, A.R., Bergamaschi, P., Niwa, Y., Segers, A., Tsuruta, A., 2020. Increasing anthropogenic methane emissions arise equally from agricultural and fossil fuel sources. Environ. Res. Lett. 15, 071002. https://doi.org/10.1088/1748-9326/ab9ed2

Janardanan, R., Maksyutov, S., Tsuruta, A., Wang, F., Tiwari, Y.K., Valsala, V., Ito, A., Yoshida, Y., Kaiser, J.W., Janssens-Maenhout, G., Arshinov, M., Sasakawa, M., Tohjima, Y., Worthy, D.E.J., Dlugokencky, E.J., Ramonet, M., Arduini, J., Lavric, J.V., Piacentino, S., Krummel, P.B., Langenfelds, R.L., Mammarella, I., Matsunaga, T., 2020. Country-Scale Analysis of Methane Emissions with a High-Resolution Inverse Model Using GOSAT and Surface Observations. Remote Sensing 12, 375. https://doi.org/10.3390/rs12030375

Jiménez-Muñoz, J.C., Mattar, C., Barichivich, J., Santamaría-Artigas, A., Takahashi, K., Malhi, Y., Sobrino, J.A., Schrier, G. van der, 2016. Record-breaking warming and extreme drought in the Amazon rainforest during the course of El Niño 2015–2016. Scientific Reports 6, 33130. https://doi.org/10.1038/srep33130

Kirschke, S., Bousquet, P., Ciais, P., Saunois, M., Canadell, J.G., Dlugokencky, E.J., Bergamaschi, P., Bergmann, D., Blake, D.R., Bruhwiler, L., Cameron-Smith, P., Castaldi, S., Chevallier, F., Feng, L., Fraser, A., Heimann, M., Hodson, E.L., Houweling, S., Josse, B., Fraser, P.J., Krummel, P.B., Lamarque, J.-F., Langenfelds, R.L., Le Quéré, C., Naik, V., O'Doherty, S., Palmer, P.I., Pison, I., Plummer, D., Poulter, B., Prinn, R.G., Rigby, M., Ringeval, B., Santini, M., Schmidt, M., Shindell, D.T., Simpson, I.J., Spahni, R., Steele, L.P., Strode, S.A., Sudo, K., Szopa, S., van der

https://doi.org/10.5194/acp-2020-1136
Preprint. Discussion started: 10 November 2020

Werf, G.R., Voulgarakis, A., van Weele, M., Weiss, R.F., Williams, J.E., Zeng, G., 2013. Three decades of global methane sources and sinks. Nature Geoscience 6, 813–823. https://doi.org/10.1038/ngeo1955

Kuze, A., Suto, H., Nakajima, M., Hamazaki, T., 2009. Thermal and near infrared sensor for carbon observation Fourier-transform spectrometer on the Greenhouse Gases Observing Satellite for greenhouse gases monitoring. Appl. Opt., AO 48, 6716–6733. https://doi.org/10.1364/AO.48.006716

Lan, X., Tans, P., Sweeney, C., Andrews, A., Dlugokencky, E., Schwietzke, S., Kofler, J., McKain, K., Thoning, K., Crotwell, M., Montzka, S., Miller, B.R., Biraud, S.C., 2019. Long-Term Measurements Show Little Evidence for Large Increases in Total U.S. Methane Emissions Over the Past Decade. Geophysical Research Letters 46, 4991–4999. https://doi.org/10.1029/2018GL081731

Lewis, S.L., Brando, P.M., Phillips, O.L., Heijden, G.M.F. van der, Nepstad, D., 2011. The 2010 Amazon Drought. Science 331, 554–554. https://doi.org/10.1126/science.1200807

McNorton, Joe, Chipperfield, M.P., Gloor, M., Wilson, C., Feng, W., Hayman, G.D., Rigby, M., Krummel, P.B., O'Doherty, S., Prinn, R.G., Weiss, R.F., Young, D., Dlugokencky, E., Montzka, S.A., 2016. Role of OH variability in the stalling of the global atmospheric CH_4 growth rate from 1999 to 2006. Atmospheric Chemistry and Physics 16, 7943–7956. https://doi.org/10.5194/acp-16-7943-2016

McNorton, J., Gloor, E., Wilson, C., Hayman, G.D., Gedney, N., Comyn-Platt, E., Marthews, T., Parker, R.J., Boesch, H., Chipperfield, M.P., 2016. Role of regional wetland emissions in atmospheric methane variability. Geophysical Research Letters 43, 11,433-11,444. https://doi.org/10.1002/2016GL070649

McNorton, J., Wilson, C., Gloor, M., Parker, R.J., Boesch, H., Feng, W., Hossaini, R., Chipperfield, M.P., 2018. Attribution of recent increases in atmospheric methane through 3-D inverse modelling. Atmospheric Chemistry and Physics 18, 18149–18168. https://doi.org/10.5194/acp-18-18149-2018

Meirink, J.F., Bergamaschi, P., Krol, M.C., 2008. Four-dimensional variational data assimilation for inverse modelling of atmospheric methane emissions: method and comparison with synthesis inversion. Atmospheric Chemistry and Physics 8, 6341–6353. https://doi.org/10.5194/acp-8-6341-2008

Melack, J.M., Hess, L.L., Gastil, M., Forsberg, B.R., Hamilton, S.K., Lima, I.B.T., Novo, E.M.L.M., 2004. Regionalization of methane emissions in the Amazon Basin with microwave remote sensing. Global Change Biology 10, 530–544. https://doi.org/10.1111/j.1365-2486.2004.00763.x

Melton, J.R., Wania, R., Hodson, E.L., Poulter, B., Ringeval, B., Spahni, R., Bohn, T., Avis, C.A., Beerling, D.J., Chen, G., Eliseev, A.V., Denisov, S.N., Hopcroft, P.O., Lettenmaier, D.P., Riley, W.J., Singarayer, J.S., Subin, Z.M., Tian, H., Zürcher, S., Brovkin, V., van Bodegom, P.M., Kleinen, T., Yu, Z.C., Kaplan, J.O., 2013. Present state of global wetland extent and wetland methane modelling: conclusions from a model inter-comparison project (WETCHIMP). Biogeosciences 10, 753–788. https://doi.org/10.5194/bg-10-753-2013

https://doi.org/10.5194/acp-2020-1136
Preprint. Discussion started: 10 November 2020

Atmospheric Chemistry and Physics Discussions

Miller, J.B., Gatti, L.V., d'Amelio, M.T.S., Crotwell, A.M., Dlugokencky, E.J., Bakwin, P., Artaxo, P., Tans, P.P., 2007. Airborne measurements indicate large methane emissions from the eastern Amazon basin. Geophysical Research Letters 34. https://doi.org/10.1029/2006GL029213

Miller, S.M., Michalak, A.M., Detmers, R.G., Hasekamp, O.P., Bruhwiler, L.M.P., Schwietzke, S., 2019. China's coal mine methane regulations have not curbed growing emissions. Nature Communications 10, 303. https://doi.org/10.1038/s41467-018-07891-7

Monks, S.A., Arnold, S.R., Hollaway, M.J., Pope, R.J., Wilson, C., Feng, W., Emmerson, K.M., Kerridge, B.J., Latter, B.L., Miles, G.M., Siddans, R., Chipperfield, M.P., 2017. The TOMCAT global chemical transport model v1.6: description of chemical mechanism and model evaluation. Geoscientific Model Development 10, 3025–3057. https://doi.org/10.5194/gmd-10-3025-2017

Monks, S.A., Wilson, C., Emmons, L.K., Hannigan, J.W., Helmig, D., Blake, N.J., Blake, D.R., 2018. Using an Inverse Model to Reconcile Differences in Simulated and Observed Global Ethane Concentrations and Trends Between 2008 and 2014. Journal of Geophysical Research: Atmospheres 123, 11,262-11,282. https://doi.org/10.1029/2017JD028112

Montzka, S.A., Krol, M., Dlugokencky, E., Hall, B., Jöckel, P., Lelieveld, J., 2011. Small Interannual Variability of Global Atmospheric Hydroxyl. Science 331, 67–69. https://doi.org/10.1126/science.119740

Murguia-Flores, F., Arndt, S., Ganesan, A.L., Murray-Tortarolo, G., Hornibrook, E.R.C., 2018. Soil Methanotrophy Model (MeMo v1.0): a process-based model to quantify global uptake of atmospheric methane by soil. Geoscientific Model Development 11, 2009–2032. https://doi.org/10.5194/gmd-11-2009-2018

Myhre, G., Shindell, D., Bréon, F.-M., Collins, W., Fuglestvedt, J., Huang, J., Koch, D., Lamarque, J.-F., Lee, D., Mendoza, B., Nakajima, T., Robock, A., Stephens, G., Zhang, H., Aamaas, B., Boucher, O., Dalsøren, S.B., Daniel, J.S., Forster, P., Granier, C., Haigh, J., Hodnebrog, Ø., Kaplan, J.O., Marston, G., Nielsen, C.J., O'Neill, B.C., Peters, G.P., Pongratz, J., Ramaswamy, V., Roth, R., Rotstayn, L., Smith, S.J., Stevenson, D., Vernier, J.-P., Wild, O., Young, P., Jacob, D., Ravishankara, A.R., Shine, K., 2013. Anthropogenic and Natural Radiative Forcing. Climate Change 2013: The Physical Science Basis. Contribution of Working Group I to the Fifth Assessment Report of the Intergovernmental Panel on Climate Change [Stocker, T.F., D. Qin, G.-K. Plattner, M. Tignor, S.K. Allen, J. Boschung, A. Nauels, Y. Xia, V. Bex and P.M. Midgley (eds.)]., Cambridge University Press, Cambridge, United Kingdom and New York, NY, USA.

Nisbet, E.G., Dlugokencky, E.J., Manning, M.R., Lowry, D., Fisher, R.E., France, J.L., Michel, S.E., Miller, J.B., White, J.W.C., Vaughn, B., Bousquet, P., Pyle, J.A., Warwick, N.J., Cain, M., Brownlow, R., Zazzeri, G., Lanoisellé, M., Manning, A.C., Gloor, E., Worthy, D.E.J., Brunke, E.-G., Labuschagne, C., Wolff, E.W., Ganesan, A.L., 2016. Rising atmospheric methane: 2007–2014 growth and isotopic shift. Global Biogeochemical Cycles 30, 1356–1370. https://doi.org/10.1002/2016GB005406

Nisbet, E.G., Manning, M.R., Dlugokencky, E.J., Fisher, R.E., Lowry, D., Michel, S.E., Myhre, C.L., Platt, S.M., Allen, G., Bousquet, P., Brownlow, R., Cain, M., France, J.L., Hermansen, O., Hossaini, R., Jones, A.E., Levin, I., Manning, A.C., Myhre, G., Pyle, J.A., Vaughn, B.H., Warwick, N.J., White, J.W.C., 2019. Very Strong Atmospheric Methane Growth in the 4 Years 2014–2017: Implications for the Paris Agreement. Global Biogeochemical Cycles 33, 318–342. https://doi.org/10.1029/2018GB006009

Nocedal, J., 1980. Updating quasi-Newton matrices with limited storage. Math. Comp. 35, 773–782. https://doi.org/10.1090/S0025-5718-1980-0572855-7

Olivier, J.G., Peters, J.A., Janssens-Maenhout, G., 2012. Trends in Global CO2 Emissions 2012 Report. PBL Netherlands Environmental Assessment Agency, Hague, Neth.

Pangala, S.R., Enrich-Prast, A., Basso, L.S., Peixoto, R.B., Bastviken, D., Hornibrook, E.R.C., Gatti, L.V., Marotta, H., Calazans, L.S.B., Sakuragui, C.M., Bastos, W.R., Malm, O., Gloor, E., Miller, J.B., Gauci, V., 2017. Large emissions from floodplain trees close the Amazon methane budget. Nature 552, 230–234. https://doi.org/10.1038/nature24639

Parker, R., Boesch, H., Cogan, A., Fraser, A., Feng, L., Palmer, P.I., Messerschmidt, J., Deutscher, N., Griffith, D.W.T., Notholt, J., Wennberg, P.O., Wunch, D., 2011. Methane observations from the Greenhouse Gases Observing SATellite: Comparison to ground-based TCCON data and model calculations. Geophysical Research Letters 38. https://doi.org/10.1029/2011GL047871

Parker, R.J., Boesch, H., McNorton, J., Comyn-Platt, E., Gloor, M., Wilson, C., Chipperfield, M.P., Hayman, G.D., Bloom, A.A., 2018. Evaluating year-to-year anomalies in tropical wetland methane emissions using satellite CH4 observations. Remote Sensing of Environment 211, 261–275. https://doi.org/10.1016/j.rse.2018.02.011

Parker, R.J., Webb, A., Boesch, H., Somkuti, P., Barrio Guillo, R., Di Noia, A., Kalaitzi, N., Anand, J., Bergamaschi, P., Chevallier, F., Palmer, P.I., Feng, L., Deutscher, N.M., Feist, D.G., Griffith, D.W.T., Hase, F., Kivi, R., Morino, I., Notholt, J., Oh, Y.-S., Ohyama, H., Petri, C., Pollard, D.F., Roehl, C., Sha, M.K., Shiomi, K., Strong, K., Sussmann, R., Te, Y., Velazco, V.A., Warneke, T., Wennberg, P.O., Wunch, D., 2020a. A Decade of GOSAT Proxy Satellite CH_4 Observations. Earth System Science Data Discussions 1–36. https://doi.org/10.5194/essd-2020-114

Parker, R.J., Wilson, C., Bloom, A.A., Comyn-Platt, E., Hayman, G., McNorton, J., Boesch, H., Chipperfield, M.P., 2020b. Exploring Constraints on a Wetland Methane Emission Ensemble (WetCHARTs) using GOSAT Satellite Observations. Biogeosciences Discussions 1–33. https://doi.org/10.5194/bg-2020-284

Patra, P.K., Houweling, S., Krol, M., Bousquet, P., Belikov, D., Bergmann, D., Bian, H., Cameron-Smith, P., Chipperfield, M.P., Corbin, K., Fortems-Cheiney, A., Fraser, A., Gloor, E., Hess, P., Ito, A., Kawa, S.R., Law, R.M., Loh, Z., Maksyutov, S., Meng, L., Palmer, P.I., Prinn, R.G., Rigby, M., Saito, R., Wilson, C., 2011. TransCom model simulations of CH_4 and related species: linking transport, surface flux and chemical loss with CH_4 variability in the troposphere and lower stratosphere. Atmospheric Chemistry and Physics 11, 12813–12837. https://doi.org/10.5194/acp-11-12813-2011

Poulter, B., Aragão, L., Heyder, U., Gumpenberger, M., Heinke, J., Langerwisch, F., Rammig, A., Thonicke, K., Cramer, W., 2010. Net biome production of the Amazon Basin in the 21st century. Global Change Biology 16, 2062–2075. https://doi.org/10.1111/j.1365-2486.2009.02064.x

Prather, M.J., Holmes, C.D., Hsu, J., 2012. Reactive greenhouse gas scenarios: Systematic exploration of uncertainties and the role of atmospheric chemistry. Geophysical Research Letters 39. https://doi.org/10.1029/2012GL051440

Randerson, J.T., Van Der Werf, G.R., Giglio, L., Collatz, G.J., Kasibhatla, P.S., 2015. Global Fire Emissions Database, Version 4.1 (GFEDv4). ORNL DAAC. https://doi.org/10.3334/ORNLDAAC/1293

Rigby, M., Montzka, S.A., Prinn, R.G., White, J.W.C., Young, D., O'Doherty, S., Lunt, M.F., Ganesan, A.L., Manning, A.J., Simmonds, P.G., Salameh, P.K., Harth, C.M., Mühle, J., Weiss, R.F., Fraser, P.J., Steele, L.P., Krummel, P.B., McCulloch, A., Park, S., 2017. Role of atmospheric oxidation in recent methane growth. Proc Natl Acad Sci USA 114, 5373–5377. https://doi.org/10.1073/pnas.1616426114

Ringeval, B., Houweling, S., van Bodegom, P.M., Spahni, R., van Beek, R., Joos, F., Röckmann, T., 2014. Methane emissions from floodplains in the Amazon Basin: challenges in developing a process-based model for global applications. Biogeosciences 11, 1519–1558. https://doi.org/10.5194/bg-11-1519-2014

Rubino, M., Etheridge, D.M., Thornton, D.P., Howden, R., Allison, C.E., Francey, R.J., Langenfelds, R.L., Steele, L.P., Trudinger, C.M., Spencer, D.A., Curran, M.A.J., van Ommen, T.D., Smith, A.M., 2019. Revised records of atmospheric trace gases CO2, CH4, N2O, and δ13C-CO2 over the last 2000 years from Law Dome, Antarctica. Earth Syst. Sci. Data 11, 473–492. https://doi.org/10.5194/essd-11-473-2019

Saunois, M., Bousquet, P., Poulter, B., Peregon, A., Ciais, P., Canadell, J.G., Dlugokencky, E.J., Etiope, G., Bastviken, D., Houweling, S., Janssens-Maenhout, G., Tubiello, F.N., Castaldi, S., Jackson, R.B., Alexe, M., Arora, V.K., Beerling, D.J., Bergamaschi, P., Blake, D.R., Brailsford, G., Brovkin, V., Bruhwiler, L., Crevoisier, C., Crill, P., Covey, K., Curry, C., Frankenberg, C., Gedney, N., Höglund-Isaksson, L., Ishizawa, M., Ito, A., Joos, F., Kim, H.-S., Kleinen, T., Krummel, P., Lamarque, J.-F., Langenfelds, R., Locatelli, R., Machida, T., Maksyutov, S., McDonald, K.C., Marshall, J., Melton, J.R., Morino, I., Naik, V., O'Doherty, S., Parmentier, F.-J.W., Patra, P.K., Peng, C., Peng, S., Peters, G.P., Pison, I., Prigent, C., Prinn, R., Ramonet, M., Riley, W.J., Saito, M., Santini, M., Schroeder, R., Simpson, I.J., Spahni, R., Steele, P., Takizawa, A., Thornton, B.F., Tian, H., Tohjima, Y., Viovy, N., Voulgarakis, A., van Weele, M., van der Werf, G.R., Weiss, R., Wiedinmyer, C., Wilton, D.J., Wiltshire, A., Worthy, D., Wunch, D., Xu, X., Yoshida, Y., Zhang, B., Zhang, Z., Zhu, Q., 2016. The global methane budget 2000–2012. Earth Syst. Sci. Data 8, 697–751. https://doi.org/10.5194/essd-8-697-2016

Saunois, M., Stavert, A.R., Poulter, B., Bousquet, P., Canadell, J.G., Jackson, R.B., Raymond, P.A., Dlugokencky, E.J., Houweling, S., Patra, P.K., Ciais, P., Arora, V.K., Bastviken, D., Bergamaschi, P., Blake, D.R., Brailsford, G., Bruhwiler, L., Carlson, K.M., Carrol, M., Castaldi, S., Chandra, N., Crevoisier, C., Crill, P.M., Covey, K., Curry, C.L., Etiope, G., Frankenberg, C., Gedney, N., Hegglin, M.I., Höglund-Isaksson, L., Hugelius, G., Ishizawa, M., Ito, A., Janssens-Maenhout, G., Jensen, K.M., Joos, F., Kleinen, T., Krummel, P.B., Langenfelds, R.L., Laruelle,

https://doi.org/10.5194/acp-2020-1136
Preprint. Discussion started: 10 November 2020

G.G., Liu, L., Machida, T., Maksyutov, S., McDonald, K.C., McNorton, J., Miller, P.A., Melton, J.R., Morino, I., Müller, J., Murguia-Flores, F., Naik, V., Niwa, Y., Noce, S., O'Doherty, S., Parker, R.J., Peng, C., Peng, S., Peters, G.P., Prigent, C., Prinn, R., Ramonet, M., Regnier, P., Riley, W.J., Rosentreter, J.A., Segers, A., Simpson, I.J., Shi, H., Smith, S.J., Steele, L.P., Thornton, B.F., Tian, H., Tohjima, Y., Tubiello, F.N., Tsuruta, A., Viovy, N., Voulgarakis, A., Weber, T.S., van Weele, M., van der Werf, G.R., Weiss, R.F., Worthy, D., Wunch, D., Yin, Y., Yoshida, Y., Zhang, W., Zhang, Z., Zhao, Y., Zheng, B., Zhu, Qing, Zhu, Qiuan, Zhuang, Q., 2020. The Global Methane Budget 2000–2017. Earth Syst. Sci. Data 12, 1561–1623. https://doi.org/10.5194/essd-12-1561-2020

Schaefer, H., 2019. On the Causes and Consequences of Recent Trends in Atmospheric Methane. Curr Clim Change Rep 5, 259–274. https://doi.org/10.1007/s40641-019-00140-z

Schaefer, H., Fletcher, S.E.M., Veidt, C., Lassey, K.R., Brailsford, G.W., Bromley, T.M., Dlugokencky, E.J., Michel, S.E., Miller, J.B., Levin, I., Lowe, D.C., Martin, R.J., Vaughn, B.H., White, J.W.C., 2016. A 21st-century shift from fossil-fuel to biogenic methane emissions indicated by 13CH4. Science 352, 80–84. https://doi.org/10.1126/science.aad2705

Shindell, D., Kuylenstierna, J.C.I., Vignati, E., Dingenen, R. van, Amann, M., Klimont, Z., Anenberg, S.C., Muller, N., Janssens-Maenhout, G., Raes, F., Schwartz, J., Faluvegi, G., Pozzoli, L., Kupiainen, K., Höglund-Isaksson, L., Emberson, L., Streets, D., Ramanathan, V., Hicks, K., Oanh, N.T.K., Milly, G., Williams, M., Demkine, V., Fowler, D., 2012. Simultaneously Mitigating Near-Term Climate Change and Improving Human Health and Food Security. Science 335, 183–189. https://doi.org/10.1126/science.1210026

Silva Junior, C.H.L., Anderson, L.O., Silva, A.L., Almeida, C.T., Dalagnol, R., Pletsch, M.A.J.S., Penha, T.V., Paloschi, R.A., Aragão, L.E.O.C., 2019. Fire Responses to the 2010 and 2015/2016 Amazonian Droughts. Front. Earth Sci. 7. https://doi.org/10.3389/feart.2019.00097

Spivakovsky, C.M., Logan, J.A., Montzka, S.A., Balkanski, Y.J., Foreman-Fowler, M., Jones, D.B.A., Horowitz, L.W., Fusco, A.C., Brenninkmeijer, C. a. M., Prather, M.J., Wofsy, S.C., McElroy, M.B., 2000. Three-dimensional climatological distribution of tropospheric OH: Update and evaluation. Journal of Geophysical Research: Atmospheres 105, 8931–8980. https://doi.org/10.1029/1999JD901006

Thompson, R.L., Lassaletta, L., Patra, P.K., Wilson, C., Wells, K.C., Gressent, A., Koffi, E.N., Chipperfield, M.P., Winiwarter, W., Davidson, E.A., Tian, H., Canadell, J.G., 2019. Acceleration of global N 2 O emissions seen from two decades of atmospheric inversion. Nature Climate Change 9, 993–998. https://doi.org/10.1038/s41558-019-0613-7

Tian, H., Xu, R., Canadell, J.G., Thompson, R.L., Winiwarter, W., Suntharalingam, P., Davidson, E.A., Ciais, P., Jackson, R.B., Janssens-Maenhout, G., Prather, M.J., Regnier, P., Pan, N., Pan, S., Peters, G.P., Shi, H., Tubiello, F.N., Zaehle, S., Zhou, F., Arneth, A., Battaglia, G., Berthet, S., Bopp, L., Bouwman, A.F., Buitenhuis, E.T., Chang, J., Chipperfield, M.P., Dangal, S.R.S., Dlugokencky, E., Elkins, J.W., Eyre, B.D., Fu, B., Hall, B., Ito, A., Joos, F., Krummel, P.B., Landolfi, A., Laruelle, G.G., Lauerwald, R., Li, W., Lienert, S., Maavara, T., MacLeod, M., Millet, D.B., Olin, S., Patra, P.K., Prinn, R.G., Raymond, P.A., Ruiz, D.J., van der Werf, G.R., Vuichard, N., Wang, J., Weiss, R.F., Wells, K.C., Wilson, C., Yang, J., Yao, Y., 2020. A comprehensive quantification of global nitrous oxide sources and sinks. Nature 586, 248–256. https://doi.org/10.1038/s41586-020-2780-0

Tunnicliffe, R.L., Ganesan, A.L., Parker, R.J., Boesch, H., Gedney, N., Poulter, B., Zhang, Z., Lavrič, J.V., Walter, D., Rigby, M., Henne, S., Young, D., O'Doherty, S., 2020. Quantifying sources of Brazil's CH_4 emissions between 2010 and 2018 from satellite data. Atmospheric Chemistry and Physics Discussions 1–40. https://doi.org/10.5194/acp-2020-438

Turner, A.J., Frankenberg, C., Wennberg, P.O., Jacob, D.J., 2017. Ambiguity in the causes for decadal trends in atmospheric methane and hydroxyl. Proc Natl Acad Sci USA 114, 5367–5372. https://doi.org/10.1073/pnas.1616020114

van der Werf, G.R., Randerson, J.T., Giglio, L., Leeuwen, T.T. van, Chen, Y., Rogers, B.M., Mu, M., Marle, M.J.E. van, Morton, D.C., Collatz, G.J., Yokelson, R.J., Kasibhatla, P.S., 2017. Global fire emissions estimates during 1997–2016. Earth System Science Data 9, 697–720. https://doi.org/10.5194/essd-9-697-2017

Webb, A.J., Bösch, H., Parker, R.J., Gatti, L.V., Gloor, E., Palmer, P.I., Basso, L.S., Chipperfield, M.P., Correia, C.S.C., Domingues, L.G., Feng, L., Gonzi, S., Miller, J.B., Warneke, T., Wilson, C., 2016. CH4 concentrations over the Amazon from GOSAT consistent with in situ vertical profile data. Journal of Geophysical Research: Atmospheres 121, 11,006-11,020. https://doi.org/10.1002/2016JD025263

Wilson, C., Chipperfield, M.P., Gloor, M., Chevallier, F., 2014. Development of a variational flux inversion system (INVICAT v1.0) using the TOMCAT chemical transport model. Geoscientific Model Development 7, 2485–2500. https://doi.org/10.5194/gmd-7-2485-2014

Wilson, C., Gloor, M., Gatti, L.V., Miller, J.B., Monks, S.A., McNorton, J., Bloom, A.A., Basso, L.S., Chipperfield, M.P., 2016. Contribution of regional sources to atmospheric methane over the Amazon Basin in 2010 and 2011. Global Biogeochemical Cycles 30, 400–420. https://doi.org/10.1002/2015GB005300

Worden, J.R., Bloom, A.A., Pandey, S., Jiang, Z., Worden, H.M., Walker, T.W., Houweling, S., Röckmann, T., 2017. Reduced biomass burning emissions reconcile conflicting estimates of the post-2006 atmospheric methane budget. Nature Communications 8, 2227. https://doi.org/10.1038/s41467-017-02246-0

Wunch, D., Toon, G.C., Blavier, J.-F.L., Washenfelder, R.A., Notholt, J., Connor, B.J., Griffith, D.W.T., Sherlock, V., Wennberg, P.O., 2011. The Total Carbon Column Observing Network. Philosophical Transactions of the Royal Society A: Mathematical, Physical and Engineering Sciences 369, 2087–2112. https://doi.org/10.1098/rsta.2010.0240

Yan, X., Akiyama, H., Yagi, K., Akimoto, H., 2009. Global estimations of the inventory and mitigation potential of methane emissions from rice cultivation conducted using the 2006 Intergovernmental Panel on Climate Change Guidelines. Global Biogeochemical Cycles 23. https://doi.org/10.1029/2008GB003299

Yin, Y., Chevallier, F., Ciais, P., Bousquet, P., Saunois, M., Zheng, B., Worden, J., Bloom, A.A., Parker, R., Jacob, D., Dlugokencky, E.J., Frankenberg, C., 2020. Accelerating methane growth rate from 2010 to 2017: leading

https://doi.org/10.5194/acp-2020-1136
Preprint. Discussion started: 10 November 2020

Atmospheric Chemistry and Physics Discussions

contributions from the tropics and East Asia. Atmospheric Chemistry and Physics Discussions 1–27. https://doi.org/10.5194/acp-2020-649

Yvon-Durocher, G., Allen, A.P., Bastviken, D., Conrad, R., Gudasz, C., St-Pierre, A., Thanh-Duc, N., del Giorgio, P.A., 2014. Methane fluxes show consistent temperature dependence across microbial to ecosystem scales. Nature 507, 488–491. https://doi.org/10.1038/nature13164